Electrochemical Energy Reviews (2018) 1:548–566
https://doi.org/10.1007/s41918-018-0019-7

REVIEW ARTICLE

Recent Progresses and Prospects of Cathode Materials for Non-aqueous Potassium-Ion Batteries

Yun-Hai Zhu[1,2,3] · Xu Yang[2] · Tao Sun[2] · Sai Wang[2,3] · Yin-Lei Zhao[2] · Jun-Min Yan[3] · Xin-Bo Zhang[1,2]

Received: 16 May 2018 / Revised: 10 August 2018 / Accepted: 6 September 2018 / Published online: 18 September 2018

Abstract
Rechargeable potassium-ion batteries (KIBs) are potential alternatives to lithium-ion batteries for application in large-scale energy storage systems due to their inexpensive and highly abundant resources. Recently, various anode materials have been investigated for use in KIBs, especially the traditional graphite anodes which have already been successfully applied in KIBs. In contrast, the appropriate cathode materials which are able to accommodate large K ions are urgently needed. In this review, a comprehensive summary of the latest advancements in cathode materials for non-aqueous KIBs in terms of capacity, cycle life and energy density will be presented, as well as K-storage mechanisms. In addition, various strategies to improve K-storage performance will be provided through combining insights from the study of material structures and properties and thus bring low-cost non-aqueous KIBs a step closer to application in sustainable large-scale energy storage systems.

Keywords Renewable energy · Electrochemical energy storage · Potassium-ion battery · Cathode material

PACS 82.45.Fk Electrodes · 88.80.F- Energy storage technologies · 88.80.f Batteries

1 Introduction

With increasing energy demands and environmental pollution caused by fossil fuel consumption, the utilization of various regenerative and clean energy sources, including wind, solar and wave, has rapidly increased over the years. However, this growing utilization of renewable energy creates a new set of challenges because the intermittent nature of such renewable resources makes direct integration into electrical grids difficult. To remedy this, the use of large-scale energy storage system (ESS) is widely considered to be an effective approach [1–3], in which ESSs can reserve and manage peak load energies from large solar power plants and wind power stations and smoothly and safely deliver stored energy into smart grids when consumption exceeds generation (schematically demonstrated in Fig. 1) [4]. In addition, various potential techniques, such as pump hydro, compressed air and fly wheel have been proposed for application in EESs [5–7], and electrochemical batteries appear to be the most promising due to appealing features such as long cycle lives, low memory effects, flexibility and simple maintenance [8–12].

Up to now, the use of lithium-ion batteries (LIBs) has evolved from portable electronics to electric/hybrid electric vehicles and has been predicted to be promising in future energy storage systems due to high energy densities [13–15]. However, most untapped lithium reserves are distributed in remote or politically sensitive areas and increasing demands on lithium resources will significantly increase LIB prices [16–18], making LIBs less cost-effective for ESSs. Because of this, researchers have recently shifted focus to batteries operating on low-cost and earth-abundant elements such as Na, K, Mg, Ca and Al (Table 1), which are extremely favorable for EESs [19–23]. And among these, potassium-ion batteries (KIBs) have generated particular interest as alternatives to LIBs because of the low standard potential of K/K^+

✉ Xin-Bo Zhang
xbzhang@ciac.ac.cn

1 Institute of Advanced Electrochemical Energy & School of Materials Science and Engineering, Xi'an University of Technology, Xi'an, Shaanxi 710048, China

2 State Key Laboratory of Rare Earth Resource Utilization, Changchun Institute of Applied Chemistry, Chinese Academy of Sciences, Changchun 130022, China

3 Key Laboratory of Automobile Materials (Jilin University), Ministry of Education, Department of Materials Science and Engineering, Jilin University, Changchun 130022, China

(−2.92 V vs. SHE) and the high abundance of potassium as a resource. Moreover, because solvated K ions possess a smaller Stokes radius, K electrolytes are characterized by higher ionic conductivities as compared with Li and Na electrolytes [24, 25]. Another advantage of KIBs is that graphite can achieve highly reversible deintercalation of K ions, meaning that KIBs are compatible with the well-established graphite anode industry in place of LIBs. And as a result of these advantages, KIBs have rapidly aroused considerable attention [26–28].

Theoretically, the operation mechanisms of KIBs present in a rocking-chair fashion, similar to that of LIBs and SIBs. During charging, K ions are extracted from the cathode and migrate to the anode through the electrolyte with an equal charge of electrons transferring from the cathode to the anode through an external circuit. And upon discharge, the opposite process occurs (schematically demonstrated in Fig. 2). To date, reversible K-ion storage in various anode materials has been identified, such as carbonaceous materials [29, 30], alloy-based materials [31, 32],

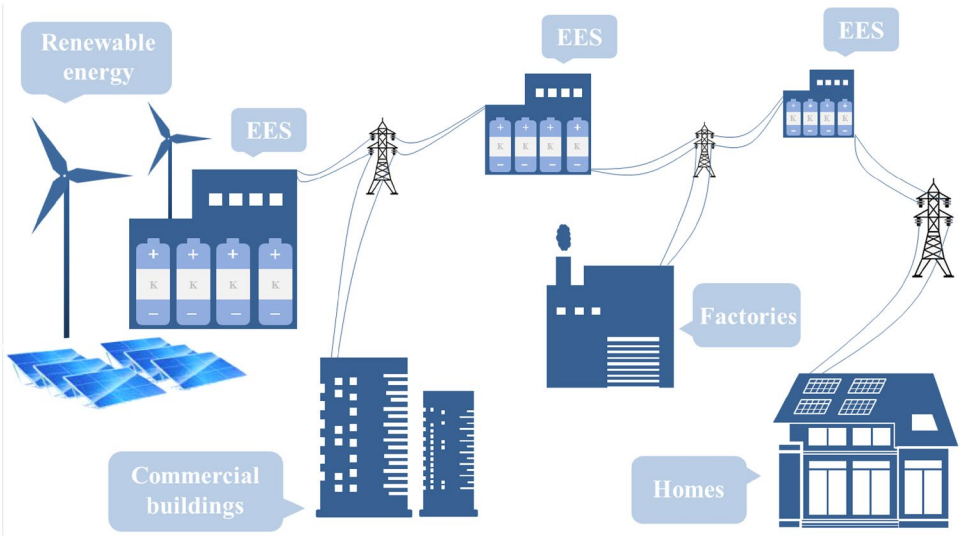

Fig. 1 Schematic illustration of the smart grid in which large-scale energy storage systems integrate renewable energy into the grid

Table 1 Comparison of the basic physical and chemical properties of Li, Na, K, Mg, Ca and Al elements

Characteristics	Li	Na	K	Mg	Ca	Al
Ionic radius (Å)	0.72	1.02	1.38	0.72	0.99	0.54
Hydrated ionic radius (Å)	3.82	3.58	3.31	4.28	4.12	4.75
Atomic mass (g mol^{-1})	6.9	23.0	39.1	24.3	40.1	27.0
Density (g cm^{-3})	0.534	0.968	0.862	1.740	1.540	2.700
Standard electrode potential (V vs. SHE)	−3.04	−2.71	−2.94	−2.37	−2.87	−1.68
Valence	+1	+1	+1	+2	+2	+3
Elemental abundance (wt%)	0.0065	2.7400	2.4700	2.0000	3.4500	7.7300
Specific capacity (mAh g^{-1})	3860	1166	685	2206	1337	2980

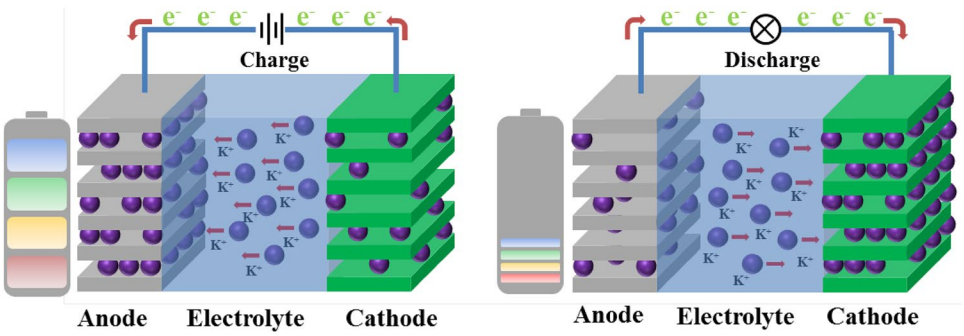

Fig. 2 Working principle of "rocking-chair" potassium-ion batteries

metal chalcogenides [33, 34] and organic materials [25, 35], and although some of these important anode materials can exhibit high capacities of about 300 mAh g^{-1}, most reported cathodes show low capacities of < 100 mAh g^{-1}, limiting the energy density of full KIBs. As a result, cathode materials largely determine the cost, specific energy and power of KIBs. In this review, ultra-modern advanced inorganic and organic cathode materials for KIBs are summarized and effective strategies to improve the performance of these materials toward EES applications are provided. Moreover, through combining ex/in situ characterizations with computational guidance, K-storage mechanisms of these materials will be discussed, providing insights for the design of new cathode materials for KIBs with improved K-storage performances.

2 Prussian Blue and Its Analogs

Prussian blue (PB) and its analogs (PBAs) are transition metal hexacyanoferrates and, in general, possess a chemical formula of $A_xM_2[M_1(CN)_6]_y{\cdot}zH_2O$ (A = alkali metal; M_1, M_2 = transition metal; $0 < x < 2$), in which high-spin M_1N_6 and low-spin M_2C_6 octahedra are alternately bridged by cyanide ligands forming a three-dimensional rigid framework (Fig. 3) [36]. In this open framework, insertion cations can occupy large "A" sites in each sub-cell and rapidly transfer along the <100> direction with little lattice strain. Given this structural advantage, PB and PBAs have been extensively investigated as new, promising cathodes for rechargeable batteries in the past several years, including SIBs, Mg-ion batteries and Ca-ion batteries [37–39]. And very recently, PB compounds have also aroused intensive attention as cathodes in KIBs because their open-framework crystal structures can enable fast insertion/extraction of relatively large K ions. In addition, PB compounds can theoretically accommodate two K-ion insertions per formula with a high theoretical capacity of approximate 155 mAh g^{-1} in cases in which both M_1 and M_2 ions are electrochemically active.

2.1 $K_xFeFe(CN)_6$

Considering their low cost and easy accessibility, iron hexacyanoferrates ($M_1 = M_2 = Fe$) are potentially superior to other PBAs as electrode candidates in KIBs and, in theory, can reversibly accommodate K ions through two types of redox reactions in which one is the oxidization of Prussian blue (PB) into Berlin green ($Fe^{III}Fe^{III}(CN)_6$; BG), and the other is the reduction of PB into Prussian white ($K_2Fe^{II}Fe^{II}(CN)_6$; PW) (Fig. 4a).

Since the first demonstration of K-ion activity for PB in a non-aqueous electrolyte by Eftekhari et al. [40], several attempts have been made to study the electrochemical properties of iron hexacyanoferrates in terms of K-ion insertion in non-aqueous systems, and recently, Zhang et al. [41] prepared PB nanoparticles using a precipitation method for evaluation in KIBs as cathode materials. Here, the researchers reported that the resulting material exhibited a reversible capacity of 73.2 mAh g^{-1} in a voltage window of 2.0~4.0 V with one discharge plateau at 3.1~3.4 V in which less than half of the K-storage sites in PB were utilized. And combined with ex situ Raman spectra, the researchers further demonstrated that only C-coordinated Fe^{III}/Fe^{II} couples were electrochemically active for K-ion storage. In a subsequent study, Chong et al. [42] investigated the electrochemical performance of the $KFe^{II}Fe^{III}(CN)_6$ cathode in the voltage range of 2.0~4.5 V and reported that two pairs of redox peaks at 3.47/3.17 V and 4.10/3.83 V can be observed (Fig. 4b), which the researchers attributed to the redox reactions of Fe^{III}/Fe^{II} redox with different spin states. And as a result of this full utilization of the different redox couples, the resulting cathode in this study achieved a high discharge capacity of 118.7 mAh g^{-1} (Fig. 4e). In addition, the researchers here indicated the K-ion extraction/insertion occurs in the $KFe^{II}Fe^{III}(CN)_6$ electrode through a mild solid solution reaction and is possibly responsible for the remarkable cycle performance.

BG is considered to possess similar electrochemical behaviors to PB in KIBs due to similar frame structures and redox couples, and in theory, a theoretical gravimetric capacity of ca. 155 mAh g^{-1}. In one example, Fu et al. [43]

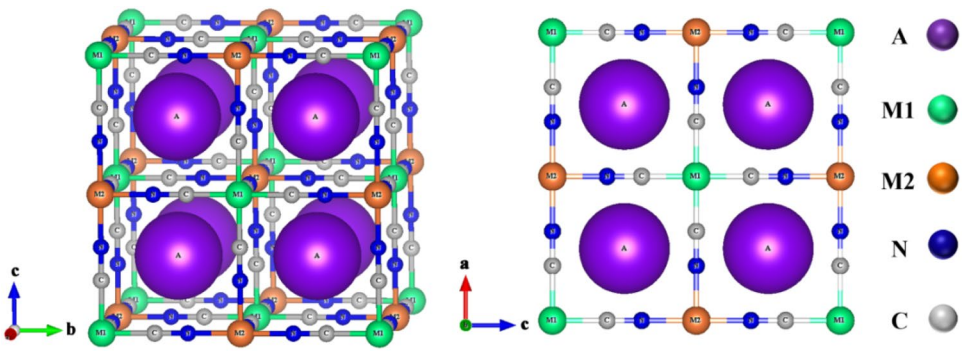

Fig. 3 Schematic crystal structures of PB and PBAs

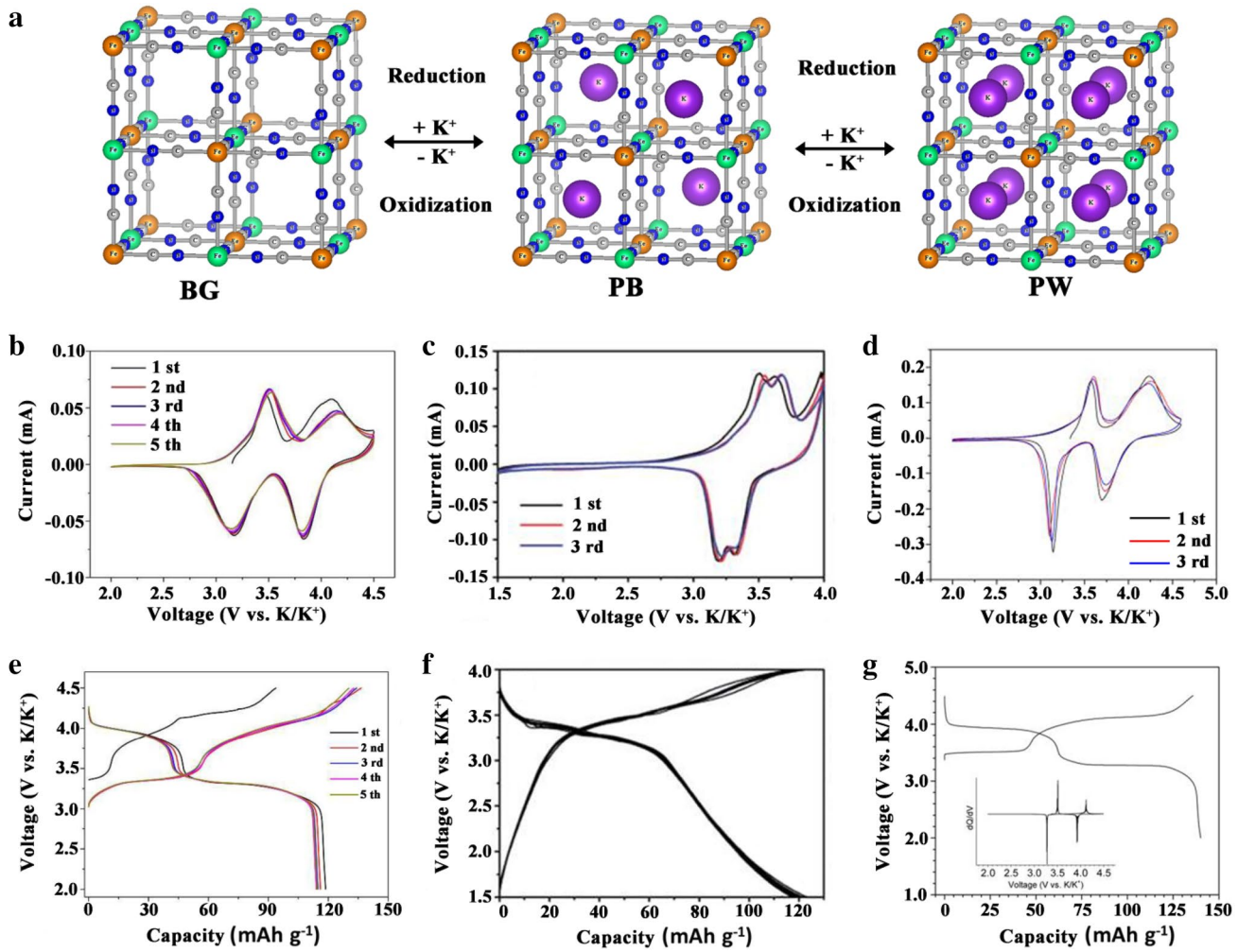

Fig. 4 **a** Schematic illustration of the redox reaction among BG, PB and PW. **b–g** Cyclic voltammograms and galvanostatic discharge/charge curves for BG (**b**, **e**), PB (**c**, **f**) and PW (**d**, **g**)

synthesized nanosized cubic BGs using a wet chemical precipitation method and evaluated its K-storage performance in non-aqueous electrolytes. Here, the researchers reported that the resulting BG electrode was capable of delivering a high reversible capacity of 124 mAh g^{-1}, corresponding to 80% of the theoretical capacity (Fig. 4f). Moreover, a reversible capacity of 93 mAh g^{-1} over 500 cycles with a coulombic efficiency of 100% was reportedly achieved, demonstrating the high reversibility of BG in terms of K insertion/extraction. Interestingly, the researchers also reported that although two pairs of redox peaks corresponding with different redox couples can be observed in the BG electrode (Fig. 4c), redox potentials (3.6/3.4 V) correlating with the low-spin Fe^{III}/Fe^{II} couple were much lower than the corresponding potentials in the PB electrode.

The reduction of PB can lead to the generation of PW, and compared with PB and BG, PW is more suitable for practical full KIBs with non-potassium metal anodes due to the high content of K. As reported by He et al. [44], PW can exhibit a high capacity of 140 mAh g^{-1} (Fig. 4g), corresponding to the insertion of 1.8 potassium ions per formula. In addition, the charge/discharge profiles obtained in this study revealed two distinct discharge plateaus, which were consistent with CV results (Fig. 4d) in which the researchers suggested that the high-potential plateau at 3.9 V originated from the low-spin Fe^{III}/Fe^{II} couple and that the low-potential plateau at 3.2 V derived from the high-spin Fe^{III}/Fe^{II} couple, demonstrating that the insertion reaction mechanism for K ions in PW is similar to that of Na ions in PBAs. This study also found that PW particle sizes have great impact on K-storage performances in which as PW particle sizes increase from 20 nm to several micrometers, capacities are reduced by tenfold (Fig. 5a–c), and that electrolytes have remarkable effects on PW electrochemical performances. Recently in another study, Liao et al. [45] demonstrated that polarization and interface impedance of PW in 1, 2-dimethoxyethane

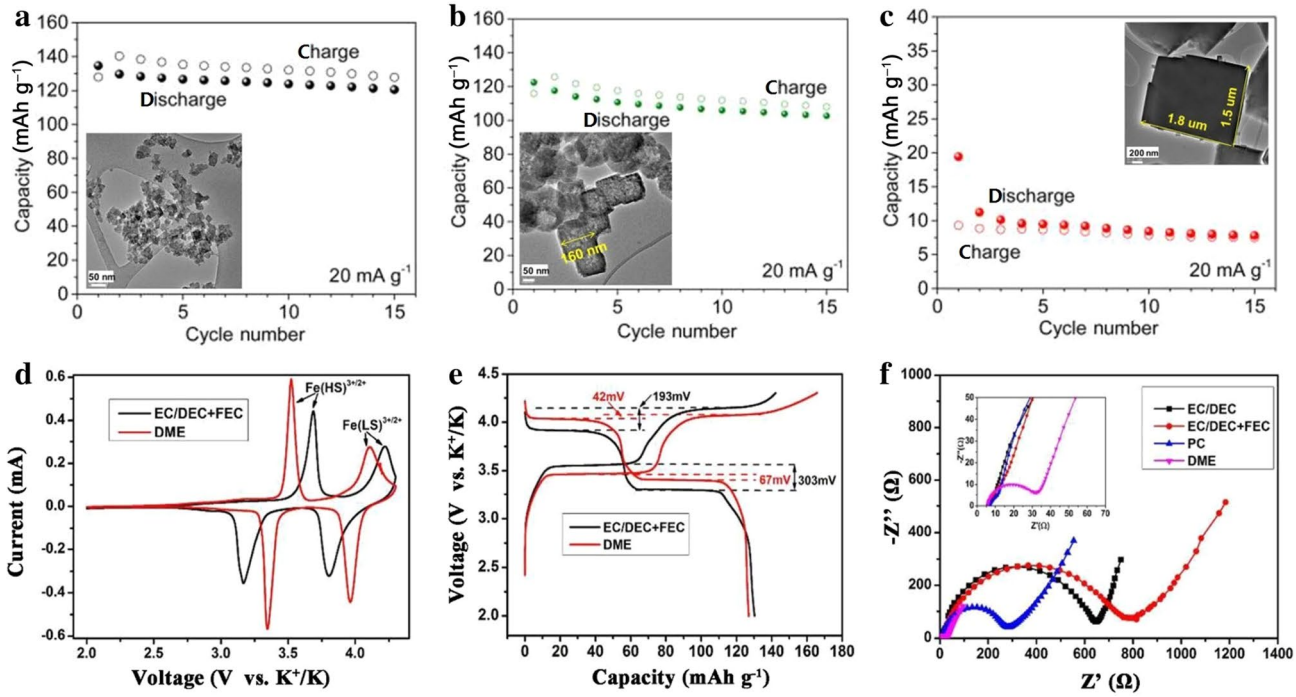

Fig. 5 **a–c** Correlation between particle size and electrochemical performance for PW at a current density of 20 mA g^{-1}. **d–f** Comparisons of CV curves, galvanostatic discharge/charge curves and EIS spectra for PW in different KPF_6-containing electrolytes

(DME)-based electrolytes were smaller than that in carbonate-based electrolytes (Fig. 5d–f), meaning that highly K-ion-conductive solid electrolyte interphase (SEI) films can be generated in DME-based electrolytes.

2.2 $K_xM_2Fe(CN)_6$ (M_2 = Mn, Co, Ni, Cu)

Manganese hexacyanoferrate is another leading candidate for KIBs applied in ESSs due to the low cost and reversible redox of Mn^{III}/Mn^{II} couples. For example, Xue et al. [46] first reported the cathode performance of $K_{1.89}Mn[Fe(CN)_6]_{0.92}\cdot 0.75H_2O$ in KIBs, in which the resulting cathode delivered a high capacity of 142 mAh g^{-1} with two flat discharge platforms at 3.56 and 3.6 V, corresponding to redox reactions of Fe^{III}/Fe^{II} and Mn^{III}/Mn^{II} redox couples, respectively. However, due to the insufficient solubility of the potassium perchlorate salt in the propylene carbonate-based electrolyte, the resulting battery tested in this study produced large polarization during the charge/discharge process. In a later study, Bie et al. [47] investigated the K-storage performance of $K_{1.75}Mn[Fe(CN)_6]_{0.93}$ in a relatively high concentration electrolyte (0.7 M potassium hexafluorophosphate in ethylene carbonate/diethyl carbonate) and reported that the $K_{1.75}Mn[Fe(CN)_6]_{0.93}$ electrode exhibited higher discharge platforms at 3.89 and 3.97 V, as well as lower polarizations (Fig. 6a). Moreover, the K-storage behaviors of this cathode were studied by using in situ XRD in which it was revealed that the electrode underwent highly reversible potassium intercalation in a topotactic manner with two two-phase reactions (Fig. 6b) and that upon K-ion extraction, the monoclinic phase first transformed into a cubic phase and subsequently into a tetragonal phase. The researchers here suggested that the first phase transition is possibly caused by the reordered arrangement of MnN_6 and FeC_6 octahedra in the crystal cell and that the subsequent phase transition is possibly from the Jahn–Teller distortion of the high-spin Mn^{3+}. Furthermore, the K-storage mechanisms of $K_2Mn[Fe(CN)_6]$ are similar to the Na insertion behaviors of hydrated $Na_2Mn[Fe(CN)_6]$ (Fig. 6c, d), and Song et al. [48] revealed that interstitial H_2O has an enormous effect on the structural and electrochemical performances of $Na_2MnFe(CN)_6\cdot zH_2O$. In this study, the researchers reported that upon removal of interstitial H_2O from hexacyanometallates, the obtained dehydrated $Na_2Mn[Fe(CN)_6]$ demonstrated a single voltage plateau (Fig. 6e), maintained 75% of initial discharge capacity over 500 cycles and was much superior to that of the hydrated one. Here, the researchers noted that the removal of the interstitial H_2O led to a phase transition of the hexacyanometallates from monoclinic to the rhombohedral phase, which in turn affected the Na-storage behaviors of the hexacyanometallates (Fig. 6f). And because the principles of KIBs are similar to SIBs, it is reasonable to assume that dehydrated hexacyanometallates can significantly improve KIB performances.

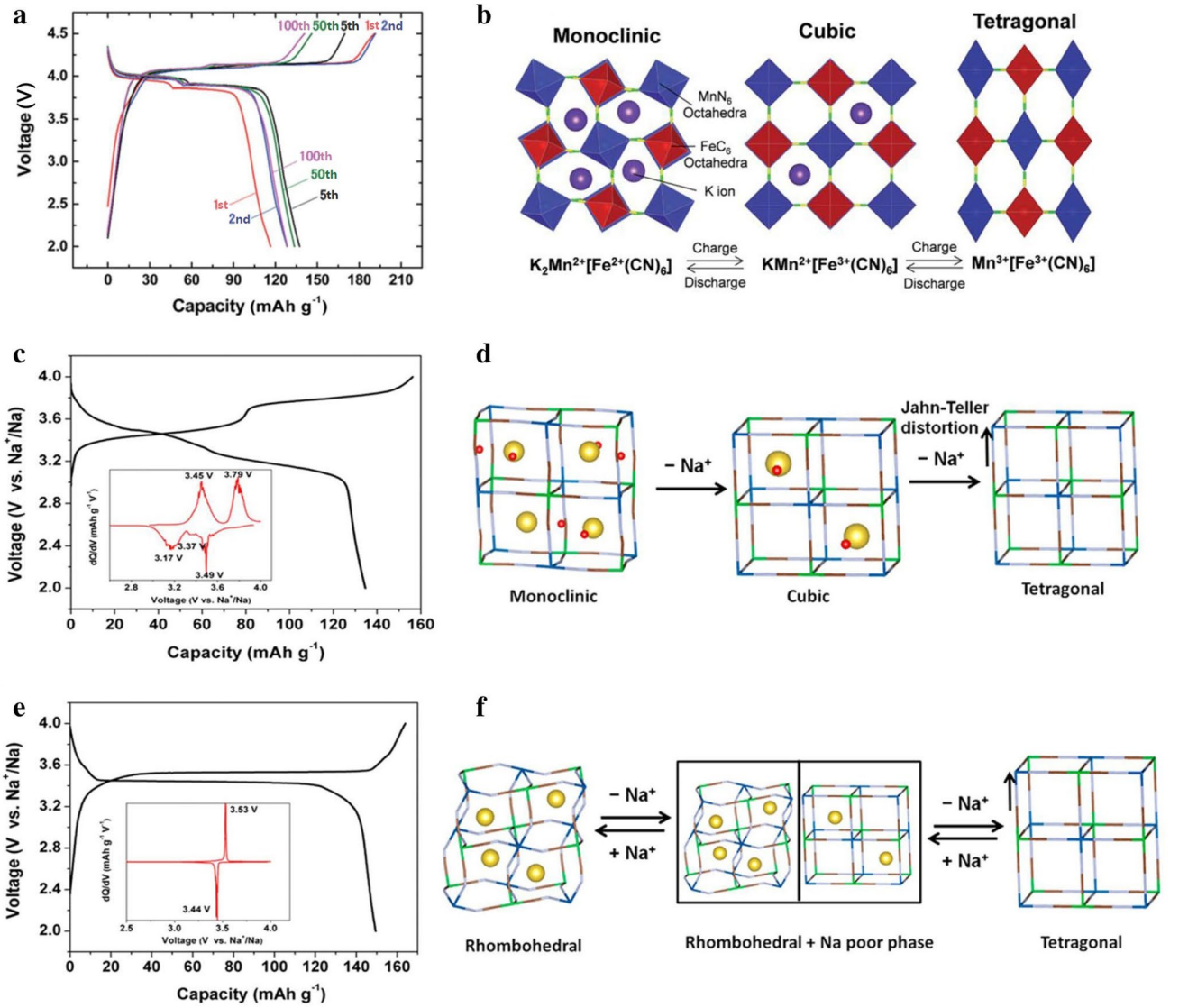

Fig. 6 Charge/discharge profiles and structural evolution of (**a**, **b**) $K_{1.75}Mn[Fe(CN)_6]_{0.93}{\cdot}0.16H_2O$ in KIBs; and charge/discharge profiles and structural evolution of (**c, d**) $Na_2MnFe(CN)_6{\cdot}zH_2O$ and (**e, f**) dehydrated $Na_2MnFe(CN)_6$ in SIBs

Other types of PBAs were also examined in KIBs by Wu et al. [49] in which all $K_2M_2Fe(CN)_6$ (M_2 = Co, Ni, Cu) were found to deliver low discharge capacities of < 65 mAh g^{-1} and were all inferior to that of $K_2FeFe(CN)_6$ and $K_2MnFe(CN)_6$ (Fig. 7). In fact, even if only a single-electron reaction occurred, the theoretical capacity of these PBAs was much higher than their obtained values and the underutilization of low-spin $Fe^{3+/2+}$ redox sites was possibly responsible for the insufficient capacity. Recently, Ren et al. [50] in their study reported a surface etching technique to facilitate the utilization of Na-storage sites in nickel hexacyanoferrate cathodes (NiHCF) and revealed that the etched NiHCF displayed unique nanoflower morphologies and possessed increased specific areas compared with unetched cathodes (Fig. 7d). And benefiting from the unique structure which maximized exposure of active sites, the etched NiHCF demonstrated full utilization of low-spin $Fe^{3+/2+}$ redox sites and delivered a capacity of ca. 90 mAh g^{-1}, which is much higher than that of unetched NiHCF (Fig. 7e, f). Overall, because K-ion diffusion is limited by the high atomic weight and large radius of K, surface activation strategies may be more effective in KIBs in terms of improving electrochemical performances.

3 Layered Oxides

As a result of controllable synthesis and high theoretical energy densities, layered transition metal oxides, $A_{1-x}MO_2$ (A = alkali, M = transition metal), have been extensively

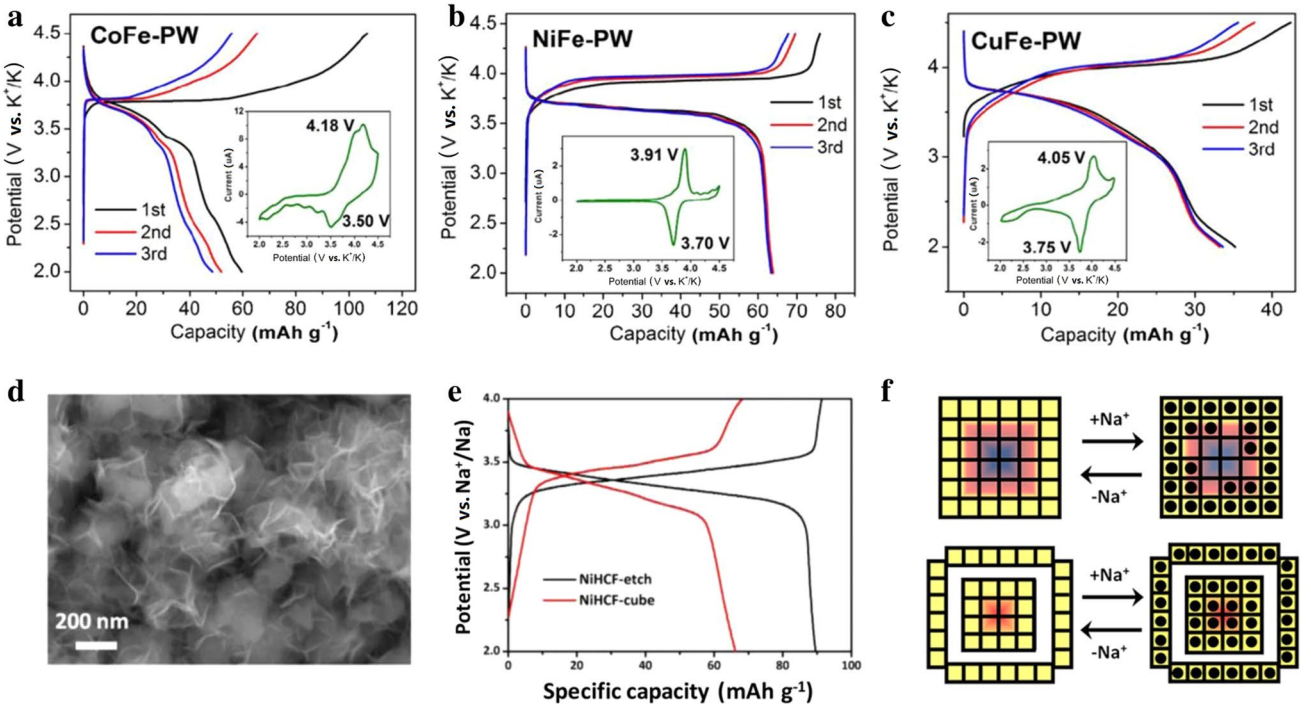

Fig. 7 **a–c** Charge/discharge profiles of $K_2CoFe(CN)_6$ (**a**), $K_2NiFe(CN)_6$ (**b**), and $K_2CuFe(CN)_6$ (**c**). **d** SEM image of the etched NiHCF. **e** Charge/discharge curves of cubic NiHCF and etched NiHCF at the second cycle. **f** Outside-in diffusion routes of Na^+ in etched NiHCF

studied in LIBs and SIBs [51, 52] and, lately, have also aroused interest from researchers as cathode materials for KIBs. In general, layered compounds can be categorized based on the stacking sequence of alkali ions between edge-shared MO_6 octahedral layers, and in theory, two main coordination environments are present for alkali ions in $A_{1-x}MO_2$, denoted as edge-shared octahedral (O) and face-shared prismatic (P) sites. Here, the number of MO_6 layers in a repetitive stacking unit is usually described with number 3 or 2. For example, P2 and P3 phases are stacked in an ABBA and ABBCCA manner with the prismatic alkali metal, and the O_3 phase is closely packed in the ABCABC pattern with the octahedral alkali metal (Fig. 8) [53, 54].

Vaalma et al. [55] first evaluated P2-type $K_{0.3}MnO_2$ (Fig. 9a) as a cathode for KIBs and reported that the resulting cathode was capable of delivering a high capacity of approximate 130 mAh g^{-1} in a voltage window of 1.5~4 V (Fig. 9d). However, the researchers also reported that because of the large volume change and layer gliding during charging above 3.5 V, this cathode possessed poor cyclability with a capacity retention of ca. 62% after 50 cycles. This was not the case if the upper limit voltage was kept to below 3.5 V however, in which the $K_{0.3}MnO_2$ cathode was able to maintain more stable cycling with capacities remaining nearly unchanged even after 50 cycles. In the subsequent studies, Hironaka et al. [56] and Kim et al.

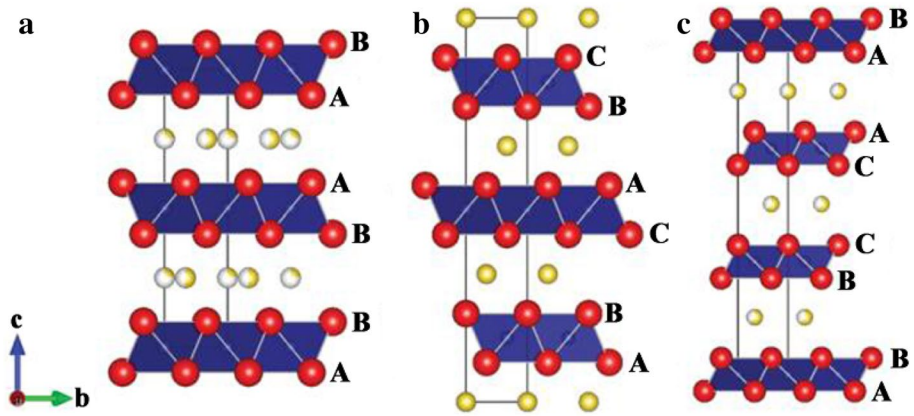

Fig. 8 **a–c** Crystal structures of P2-type (**a**), O3-type (**b**) and P3-type (**c**) layered metal oxides

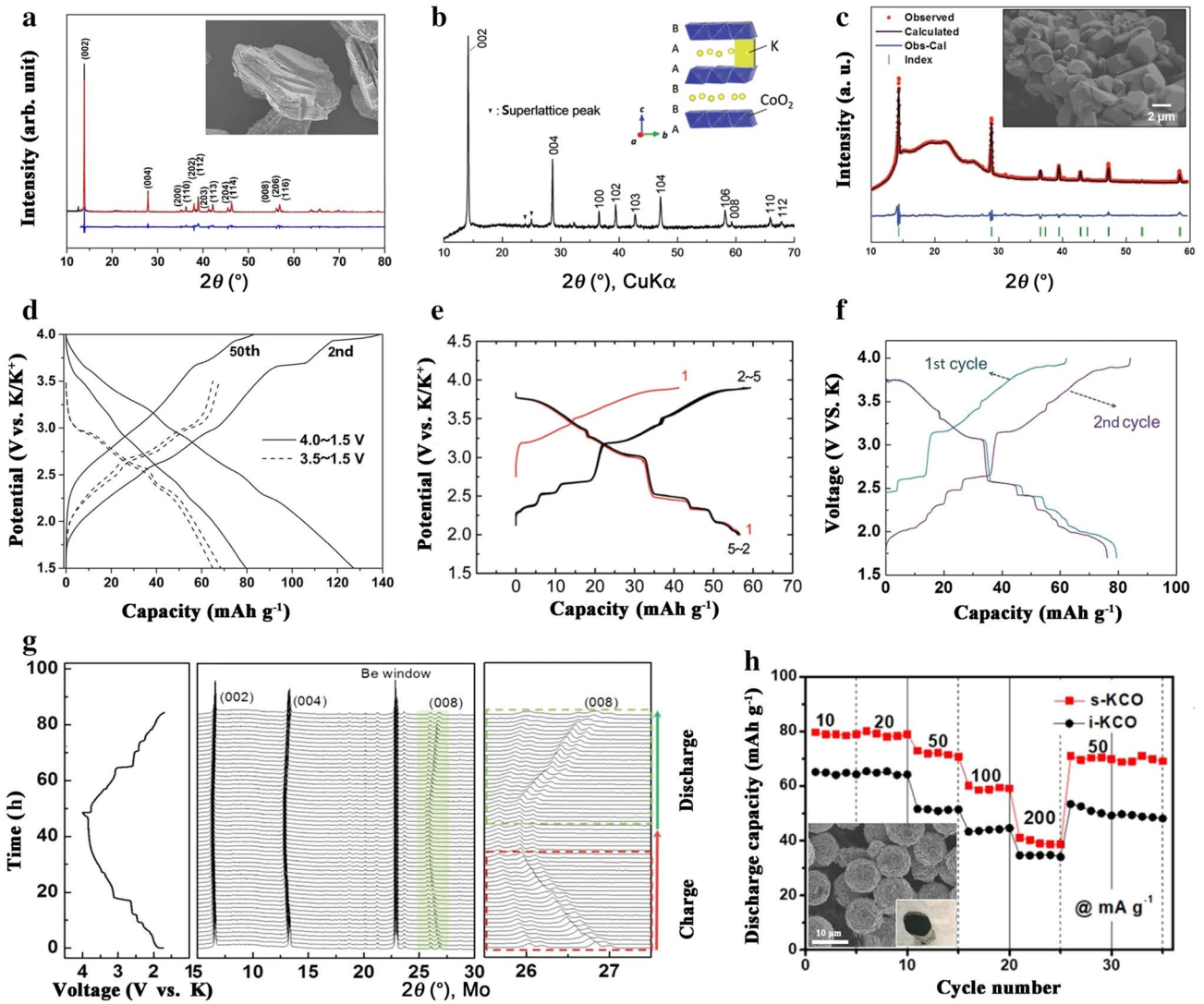

Fig. 9 Electrochemical behavior of P2-type layered metal oxides: XRD patterns and charge/discharge curves for $K_{0.3}MnO_2$ (**a**, **c**), $K_{0.41}CoO_2$ (**b**, **e**) and $K_{0.6}CoO_2$ (**c**, **f**). **g** In situ XRD characterization of P2-type $K_{0.6}CoO_2$ upon charge/discharge. **h** Rate performance of spherical $K_{0.6}CoO_2$ and irregular $K_{0.6}CoO_2$ at a constant current of 40 mA g^{-1}

[57] demonstrated that P2-type $K_{0.41}CoO_2$ (Fig. 9b) and $K_{0.6}CoO_2$ (Fig. 9c) were desired hosts for the insertion of K ions, in which $K_{0.41}CoO_2$ and $K_{0.6}CoO_2$ electrodes were capable of delivering reversible capacities of 60 mAh g^{-1} and 80 mAh g^{-1}, respectively (Fig. 9e, f). In these studies, the researchers noted that both $K_{0.41}CoO_2$ and $K_{0.6}CoO_2$ electrodes exhibited similar stair-like charge/discharge curves, demonstrating analogous K-storage mechanisms and that the different reversible capacities were possibly due to the diverse test voltage range. In addition, in situ XRD patterns of the P2-$K_{0.6}CoO_2$ electrode upon charge/discharge (Fig. 9g) revealed that during the charge process, the peak of the (008) face moves to lower angles, indicating the expansion of the crystal structure along the c-axis, possibly caused by the increased coulombic repulsion between the oxygen layers from the removal of K ions. During the discharge process, the peak of the (008) face moves back to its original position, demonstrating the reversibility of the insertion/extraction of K ions. Additionally, different degrees of shifting and asymmetric peak evolution for the (008) peak were observed, suggesting that $K_{0.6}CoO_2$ undergoes multiple phase transitions upon K-ion insertion/extraction. Here, these authors suggested that the various phase transitions originated from K-ion/vacancy ordering.

Fabricating hierarchical structures is an effective approach to promote the diffusion kinetics of inserted ions, thereby improving the electrochemical performance of transition metal oxides in LIBs and SIBs [58, 59]. Recently, Deng et al. [60] synthesized P2-type $K_{0.6}CoO_2$ hierarchical microspheres and evaluated them as cathodes in KIBs.

And because hierarchical structures enable fast kinetics for inserted K ions and reduce parasitic reactions originating from the electrolyte, the capacity and rate performance of the spherical $K_{0.6}CoO_2$ was reported to be higher and better than that of irregular $K_{0.6}CoO_2$ (Fig. 9h). More importantly, the spherical $K_{0.6}CoO_2$ was also reported to exhibit superior cycling performances, retaining nearly 87% of the initial capacity after 300 cycles. In contrast, the cycling stability of the irregular $K_{0.6}CoO_2$ cathode was inferior, retaining < 50% of the initial capacity after 100 cycles.

P3-type $K_{0.67}CoO_2$ (Fig. 10a) was first studied in non-aqueous KIBs by Hironaka et al. [56], who reported that the material was capable of delivering a reversible capacity of ca. 60 mAh g^{-1} in a voltage window of 2.0~3.9 V and demonstrating good cycle stability, with nearly unchanged capacities over 20 cycles (Fig. 10d). Subsequently, Liu et al. [61] synthesized $K_{0.67}Ni_{0.17}Co_{0.17}Mn_{0.66}O_2$ (Fig. 10b) using a co-precipitation-assisted solid-state reaction and reported that the resulting material exhibited a reversible capacity of 76.5 mAh g^{-1} in the voltage range of 2.0~4.3 V (Fig. 10e). And very recently, a new cathode material, P3-structured $K_{0.5}MnO_2$ (*R3m* space group; Fig. 10c), was employed in KIBs by Kim et al. [62], who reported that the material could deliver a reversible capacity of approximately 100 mAh g^{-1} in the voltage window of 1.5~3.9 V and maintain 81% of its origin capacity after 20 cycles (Fig. 10f). Here, the researchers noted that the original capacity of the P3-$K_{0.5}MnO_2$ can reach a very high level of 140 mAh g^{-1}

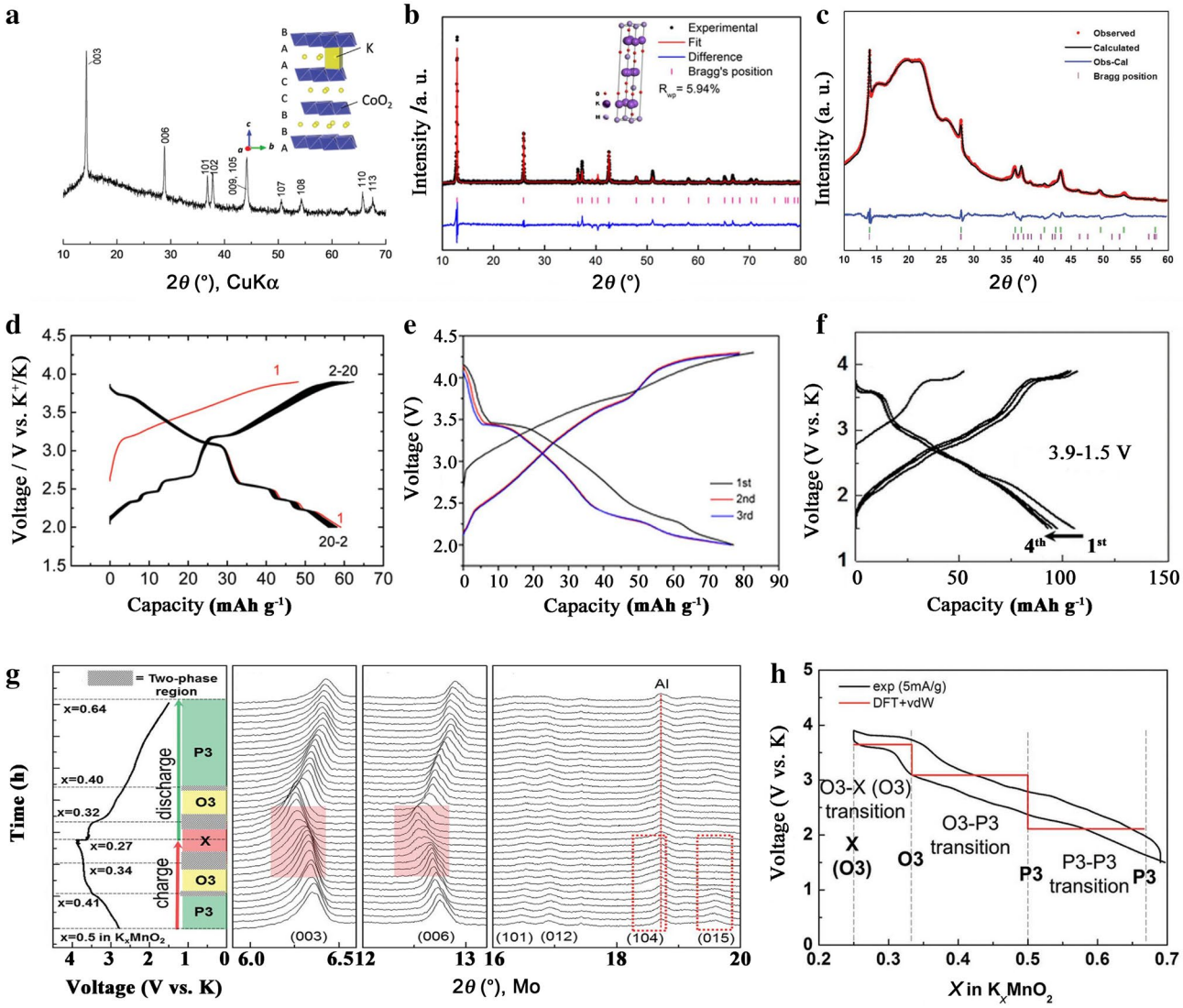

Fig. 10 Electrochemical behavior of P3-type layered metal oxides: XRD patterns and charge/discharge curves for $K_{0.67}CoO_2$ (**a**, **d**), $K_{0.67}Ni_{0.17}Co_{0.17}Mn_{0.66}O_2$ (**b**, **e**) and $K_{0.5}MnO_2$ (**c**, **f**). **g** In situ XRD characterization of P3-type $K_{0.5}MnO_2$ upon charge/discharge. **h** Calculated voltage plot (DFT + vdW) compared with experimentally obtained charge/discharge profiles of P3-type $K_{0.5}MnO_2$

if the upper cutoff potential was up to 4.2 V. However, this increased capacity did come at the expense of cycling performance, in which only 30% of its original discharge capacity could be preserved after 20 cycles in the voltage range of 1.5~4.2 V. The researchers in this study claimed that this inferior cycle stability might be caused by an irreversible structural change that occurs in the high-voltage region above 4.0 V. In addition, in situ XRD patterns of the P3-$K_{0.5}MnO_2$ cathode during cycling revealed that upon charging, this material undergoes two reversible phase transitions: P_3 to O_3 phase and O_3 to an unknown phase, and that upon discharging, the phase evolution process is totally reversed, demonstrating reversible K intercalation/deintercalation behaviors in P3-$K_{0.5}MnO_2$ (Fig. 10g). Moreover, combined with first-principles calculations, the researchers calculated the voltage profile of K_xMnO_2 as a function of K content and found that the voltage profile calculated by DFT calculations was consistent with experimental voltage profiles (Fig. 10h), further confirming the phase transition mechanisms of P3-$K_{0.5}MnO_2$.

4 Polyanionic Compounds

Owing to the strong inductive effects originating from electronegative anion groups, polyanionic compounds always possess high structural and thermodynamic stability, as well as high operating voltages. Thus, polyanions materials such as phosphates, sulfates and pyrophosphates have been widely applied in LIBs and SIBs cathodes [63–66]. And because polyanionic frameworks can better shield K–K repulsion, polyanionic compounds are promising cathode materials for KIBs as well. And currently, available polyanionic compounds such as $FeSO_4F$ [67], $FePO_4$ [68], $K_3V_2(PO_4)_3$ [69], $KVPO_4F$ [70], $KVOPO_4$ [70], $K_3V_2(PO_4)_2F_3$ [71] and KVP_2O_7 [72] are being investigated as cathodes for KIBs.

For example, Recham et al. [67] were the first to report that fluorosulfates ($FeSO_4F$) can reversibly intercalate Li, Na and K. In their study, the researchers prepared $FeSO_4F$ through the electrochemical extraction of K ions from $KFeSO_4F$ in Li/$KFeSO_4F$ cells and tested its electrochemical properties in LIBs, SIBs and KIBs, and reported that the obtained $FeSO_4F$ could accommodate approximately 0.9 Li ions, 0.85 Na ions and 0.8 K ions per formula. Interestingly, this study also reported that $FeSO_4F$ provided more pronounced voltage steps in KIBs, demonstrating the formation of multiple stable intermediate phases upon large K-ion insertion/extraction. In another study, Mathew et al. [68] reported that amorphous $FePO_4$ can reversibly intercalate various cations, including Li, Na, K, Mg and Zn ions, and suggested that the amorphous structure characterized by short-range ordering can accelerate the insertion of guest ions even at large sizes. And as a result, the researchers here reported that the amorphous $FePO_4$ delivered a high capacity of approximate 150 mAh g^{-1} upon K-ion insertion (Fig. 11a). Interestingly, ex situ XRD results revealed the transition from amorphous-to-crystalline structure upon K-ion insertion and that at the end of discharge, a new crystal phase of $KFe_2(PO_4)_2$ was generated (Fig. 11b). In addition, after being fully charged, the amorphous phase reformed, demonstrating the high reversibility of the K/$FePO_4$ cells.

Recently, carbon-confined $K_3V_2(PO_4)_3$ with a 3D porous structure was synthesized by Han et al. [69], who investigated its performance in KIBs for the first time and reported that the as-prepared $K_3V_2(PO_4)_3$ cathode can deliver a reversible capacity of approximate 54 mAh g^{-1} in the voltage range of 2.5~4.3 V and exhibit a high-potential plateau of 3.6~3.9 V (Fig. 11c). Subsequently, Chihara et al. [70] synthesized and investigated $KVPO_4F$ and $KVOPO_4$ as new cathode materials for KIBs, and reported that the $KVPO_4F$ and $KVOPO_4$ electrodes can deliver reversible capacities of approximate 92 mAh g^{-1} and 84 mAh g^{-1}, respectively (Fig. 11d–e), and that although they were isostructural to orthorhombic $KTiOPO_4$, the different redox couples of $KVPO_4F$ and $KVOPO_4$ (V^{3+}/V^{4+} for $KVPO_4F$; V^{4+}/V^{5+} for $KVOPO_4$) can lead to distinct electrochemical behaviors. Notably, Park et al. [73] suggested that due to the higher electronegativity of F atoms than O atoms, the average discharge voltage of $KVPO_4F$ (4.13 V) should be higher than that of $KVOPO_4$ (4.00 V), and that both $KVPO_4F$ and $KVOPO_4$ exhibit low coulombic efficiencies and large irreversible capacities mainly as a result of severe electrolyte decomposition upon high voltage. Here, an effective method to overcome this issue is to develop electrochemically stable electrolytes with wide voltage windows of over 4 V.

More recently, Lin et al. [71] synthesized $K_3V_2(PO_4)_2F_3$ using a similar strategy to that of Recham et al. [67] in which a Na ion was electrochemically replaced by a K ion in $Na_3V_2(PO_4)_2F_3$ to generate $K_3V_2(PO_4)_2F_3$ in a K/$Na_3V_2(PO_4)_2F_3$ cell, and investigated it as a cathode for KIBs in a voltage range of 2~4.5 V. Here, the researchers reported that the as-prepared $K_3V_2(PO_4)_2F_3$ electrode exhibited a reversible capacity of approximate 100 mAh g^{-1} with an average voltage of 3.7 V (Fig. 11f). And by combining in situ XRD with the corresponding Rietveld refinement, the authors were also able to clearly identity the structural evolution of $K_3V_2(PO_4)_2F_3$ during K-ion insertion/extraction, in which upon K-ion extraction, orthorhombic $K_3V_2(PO_4)_2F_3$ (space group *Cmcm*) first transforms to tetragonal $K_2V_2(PO_4)_2F_3$ (space group *I4/mmm*) at the low-voltage plateau and further transforms to orthorhombic $K_1V_2(PO_4)_2F_3$ (space group *Cmc21*) at the end of charge (Fig. 11g). The researchers also noted that the total volumetric change rate of $K_3V_2(PO_4)_2F_3$ was only 6.2% ($\Delta V/V$) during the charge/discharge process, demonstrating the stability of the $K_3V_2(PO_4)_2F_3$ for long-term cycles. Despite

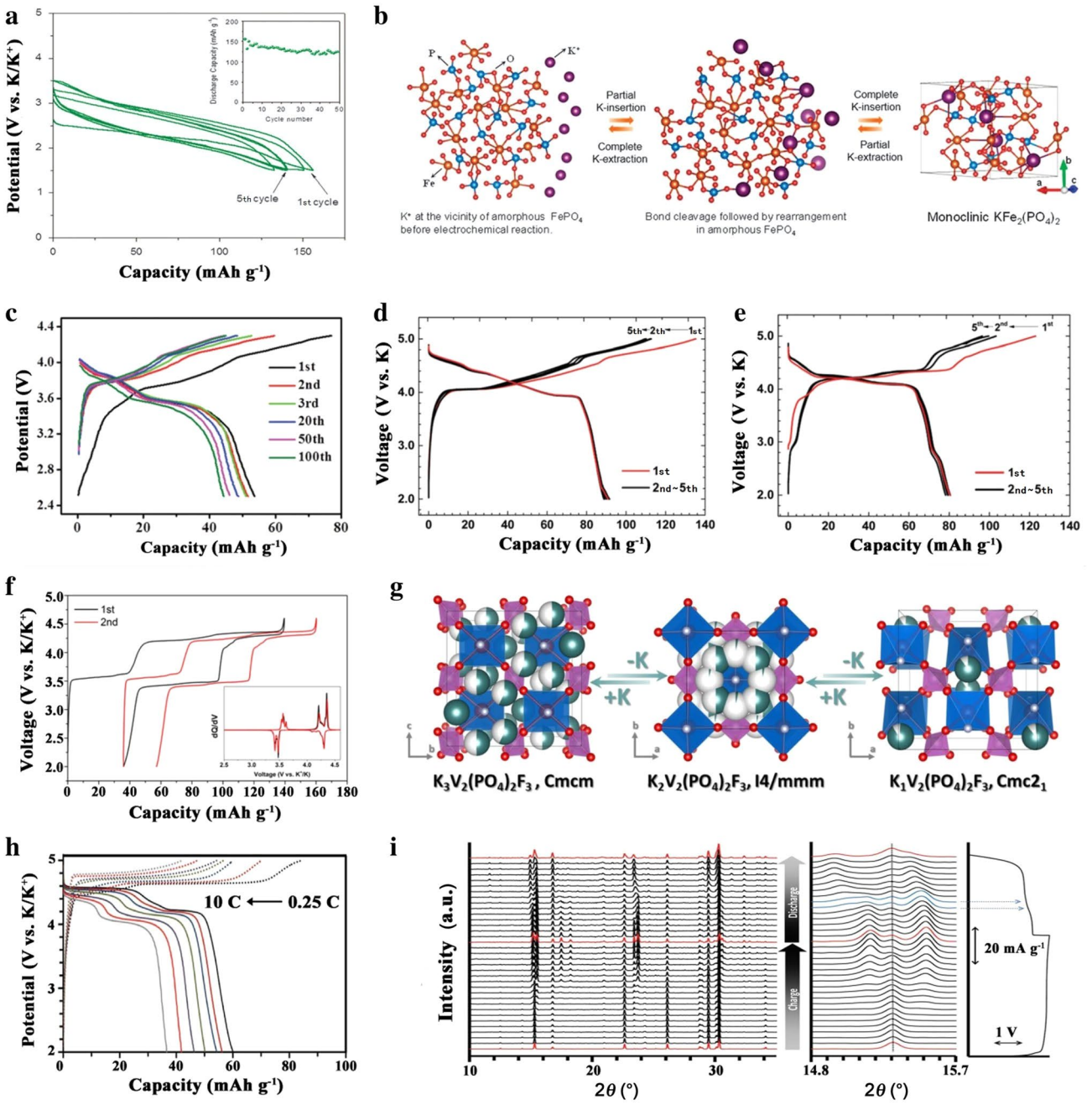

Fig. 11 **a** Initial five charge/discharge profiles of amorphous $FePO_4$. **b** Schematic illustration of the reversible amorphous-to-crystalline transition in amorphous $FePO_4$. **c** Different discharge/charge curves of $K_3V_2(PO_4)_3$/C. **d**–**e** Typical charge/discharge profiles of $KVPO_4F$ (**d**) and $KVOPO_4$ (**e**). **f** Voltage profiles of $K_3V_2(PO_4)_2F_3$ in the initial two cycles. **d** Phase transformation of $K_3V_2(PO_4)_2F_3$ during K-ion insertion and extraction. **h** Charge/discharge profiles of KVP_2O_7 at various rates. **i** In situ XRD of KVP_2O_7 during a full charge/discharge cycle

these promising results however, the resulting $K_3V_2(PO_4)_2F_3$ also exhibited disappointing rate performances, with <20 mAh g^{-1} capacity being preserved at moderate current densities (500 mA g^{-1}). The researchers in this study attributed this poor rate capability to the large size and poor electronic conductivity of $K_3V_2(PO_4)_2F_3$ (ca. 2 μm), but stated that there is possibility for improvement through the reduction in particle sizes or the construction of surface coating structures.

Furthermore, Park et al. [72] were able to pinpoint among numerous inorganic compounds that monoclinic KVP_2O_7 is a promising high energy density cathode in

non-aqueous KIBs using theoretical calculations and electrochemical validations. And in their study, the researchers reported that KVP_2O_7 exhibited a reversible capacity of approximate 60 mAh g^{-1} with an average working potential of approximate 4.2 V (Fig. 11h). This average working voltage for KVP_2O_7 is the highest among reported cathode materials to date and is of great significance for the improvement of full KIB energy densities. Moreover, the researchers also reported that this cathode was able to provide superior rate capabilities in which even at an ultrahigh current density of 1 A g^{-1}, a reversible capacity of 37 mAh g^{-1} can be obtained. Furthermore, the K-storage mechanisms of KVP_2O_7 were also investigated by using in situ XRD in this study and revealed that monoclinic KVP_2O_7 (space group *P21/c*) gradually transforms into triclinic $K_{1-x}VP_2O_7$ (space group *P1*) upon charge and recovers back to monoclinic KVP_2O_7 after discharge (Fig. 11i).

5 Organic Cathodes

Due to low costs as well as lightweight and flexible structures, organic compounds are very attractive for the fabrication of green rechargeable batteries. And up to now, various organic materials have been extensively studied in rechargeable batteries, such as radical compounds, carbonyl compounds and functional polymers [74–77]. However, because this area of research is still in its infancy, few organic electrode materials for KIBs have been successfully demonstrated.

As an organic pigment, 3,4,9,10-perylenetetracarboxylicacid-dianhydride (PTCDA) has been already studied in LIBs, SIBs and hydronium-ion batteries [78–81], and recently, Chen et al. [82] tested and verified the electrochemical performance of PTCDA in non-aqueous KIBs. In this study, the resulting organic electrode delivered a high

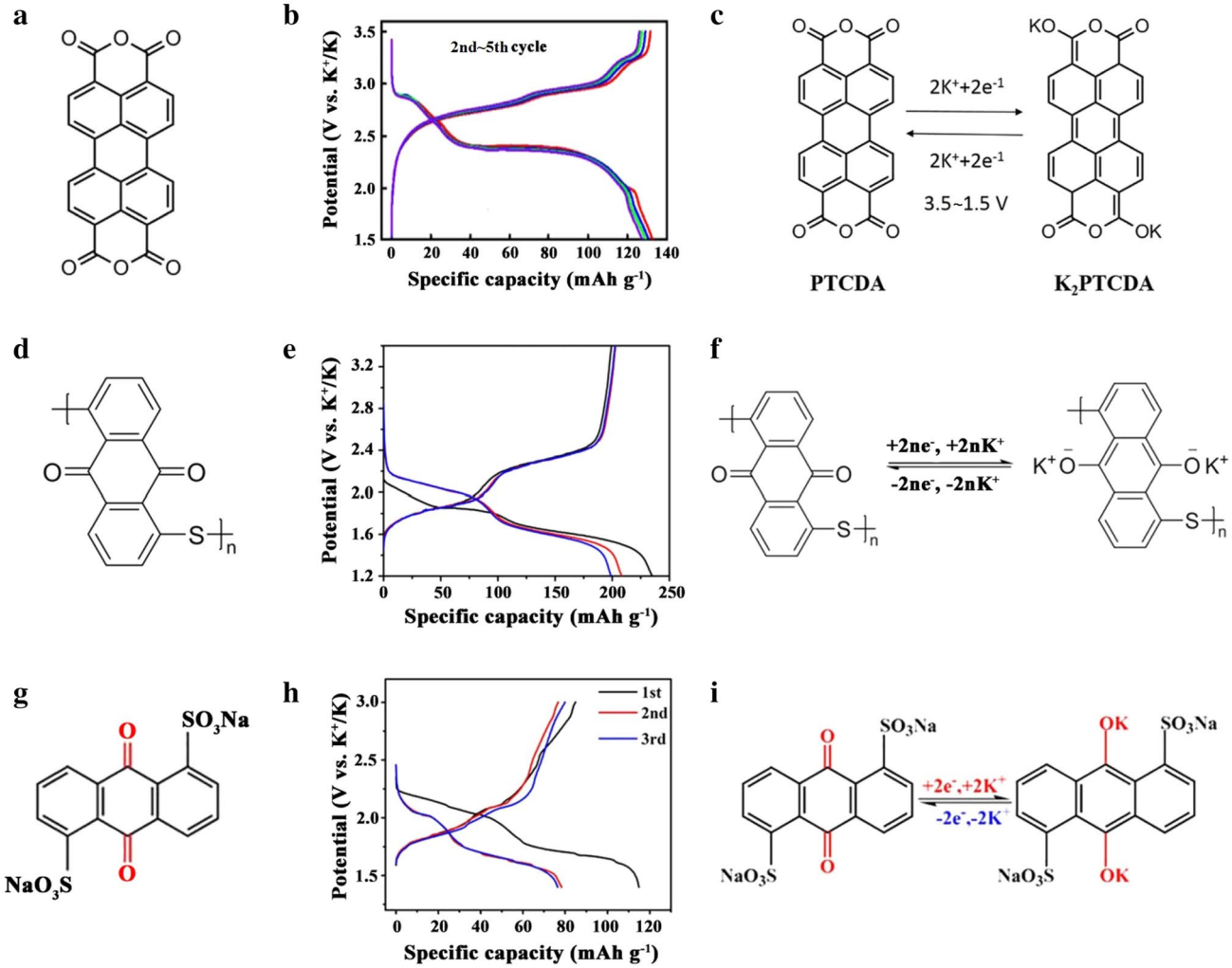

Fig. 12 Molecular structures, charge/discharge profiles and potassium storage mechanisms for **a–c** PCDTA; **d–f** PAQS; and **g–i** AQDS

reversible capacity of 131 mAh g^{-1} in the voltage range of 1.5~3.5 V (Fig. 12b), corresponding to the accommodation of two K ions per formula (Fig. 12c). Additionally, this cathode also demonstrated excellent cycling performances, retaining 66.1% of the original capacity after 200 cycles. Furthermore, the researchers reported that another 9 K ions can be accommodated by the PTCDA electrode in the voltage range of 0.01~1.5 V, suggesting its promising applications as high-capacity anodes in KIBs.

Anthraquinone (AQ)-based compounds have also been investigated in LIBs and SIBs [83–86] and are expected to be viable as cathodes in KIBs. In general, AQ compounds exhibit poor cycling stabilities because of high solubility in organic electrolytes. However, in theory, the utilization of polymers or salt formations is an effective method to solve the issue of the dissolution of small organic molecules [87, 88], and recently, Jian et al. [89] reported the use of poly(anthraquinonyl sulfide) (PAQS), an AQ-based polymer, as a cathode material in KIBs. Here, the researchers reported that the PAQS electrode exhibited a high reversible capacity of 200 mAh g^{-1} with two distinct voltage slopes in the voltage range of 1.2~3.4 V (Fig. 12e), indicating the insertion of two sequential K ions upon discharge (Fig. 12f). In a subsequent study to suppress the dissolution of AQ molecules in organic electrolytes, Zhao et al. [90] synthesized anthraquinone-1,5-disulfonic acid sodium salt (AQDS) containing polar sodium sulfonate function groups and reported that as a result, the obtained AQDS was capable of delivering excellent K-storage performances in non-aqueous KIBs (Fig. 12h), including a high reversible capacity (95 mAh g^{-1}) and a long cycle stability (maintaining 78 mAh g^{-1} after 100 cycles). In addition, in the study by Zhao et al. [90], FTIR and ex situ XRD characterizations were employed to examine the K-storage mechanism of AQDS, which confirmed that carbonyl groups in AQDS are responsible for K-ion storage (Fig. 12i).

6 Architectural Designs for Cathodes

Although the viability of various cathode materials such as PBAs, layered metal oxides, and polyanionic compounds has been successfully demonstrated in KIBs, the insertion/extraction of significantly larger K ions (0.138 nm) can cause great change in host structures, often leading to decreased cycling performance or even complete electrochemical inactivity for host materials [91, 92]. Here, studies have reported that reducing particle sizes or compositing with conductive carbon/polymers can significantly improve electrochemical performances of active materials due to enhanced electronic/ionic transport kinetics [90–94]. Generally, nanomorphology can enhance the electrochemical performance of electrode materials through the enabling of benefits such as larger surface-to-volume ratios, facile strain relaxation during battery operation, and shorter diffusion distances for both ions and electrons [95, 96]. However, because of high surface energies, nanomaterials suffer from severe agglomeration during the charge/discharge process, in particular if large K ions are embedded. Here, the use of conductive carbon-coated/supported nanocomposites is considered to be an efficient method to achieve high performance in nanocomposites, in which coated carbons can provide facile transport pathways for electrons and prevent agglomeration of active materials.

For example, Zhu et al. [97] recently fabricated a binder-free PB electrode using generated PB nanocubes on the surface of stainless-steel mesh (SSM) followed by coating with reduced graphite oxide (RGO) and reported that the resulting electrode, denoted as RGO@PB@SSM (Fig. 13a), possessed a rough surface in which cubic PB particles were in close contact with the SSM substrate and the RGO-coated layer, enabling ultrafast transport for electrons and avoiding the agglomeration and detachment of PB nanocubes upon insertion/extraction of K ions (Fig. 13b). And as a result, the researchers reported that the obtained RGO@PB@SSM electrode exhibited a high capacity of 96.8 mAh g^{-1} in the voltage range of 2~4.0 V (Fig. 13c) and maintained approximately 75.1% of its initial capacity even after 305 cycles. Subsequently, Wang et al. [98] designed and synthesized novel interconnected $K_{0.7}Mn_{0.5}Fe_{0.5}O_2$ nanowires in which $K_{0.7}Mn_{0.5}Fe_{0.5}O_2$ nanocrystallines were uniformly encapsulated in a carbon substrate (Fig. 13d) and reported that the resulting three-dimensional network enabled the fast transport of electrons and K ions, whereas the carbon substrate prevented structural failure and agglomeration of the $K_{0.7}Mn_{0.5}Fe_{0.5}O_2$ nanocrystallines during the charge/discharge process, leading to long cycling stability in KIBs. In addition, this cathode also delivered a high reversible capacity of approximate 178 mAh g^{-1} in the voltage window of 1.5~4.0 V and retained approximately 76% of the initial capacity over 250 cycles (Fig. 13e).

7 Conclusion and Outlook

Great progress has been achieved in non-aqueous KIBs, and a variety of K-storage cathodes have been successfully demonstrated. Figure 14 and Table 2 present the performance of typical cathode materials in KIBs in terms of specific capacity, average working potential and energy density, as well as cycling and rate performances, and currently, PBAs have been proven to be the most promising cathodes for large-scale KIBs due to their high capacity, great reversibility, as well as facile and scalable preparation. However, due to the decomposition of structural water upon charging, coulombic efficiencies of such materials are low, impeding their further

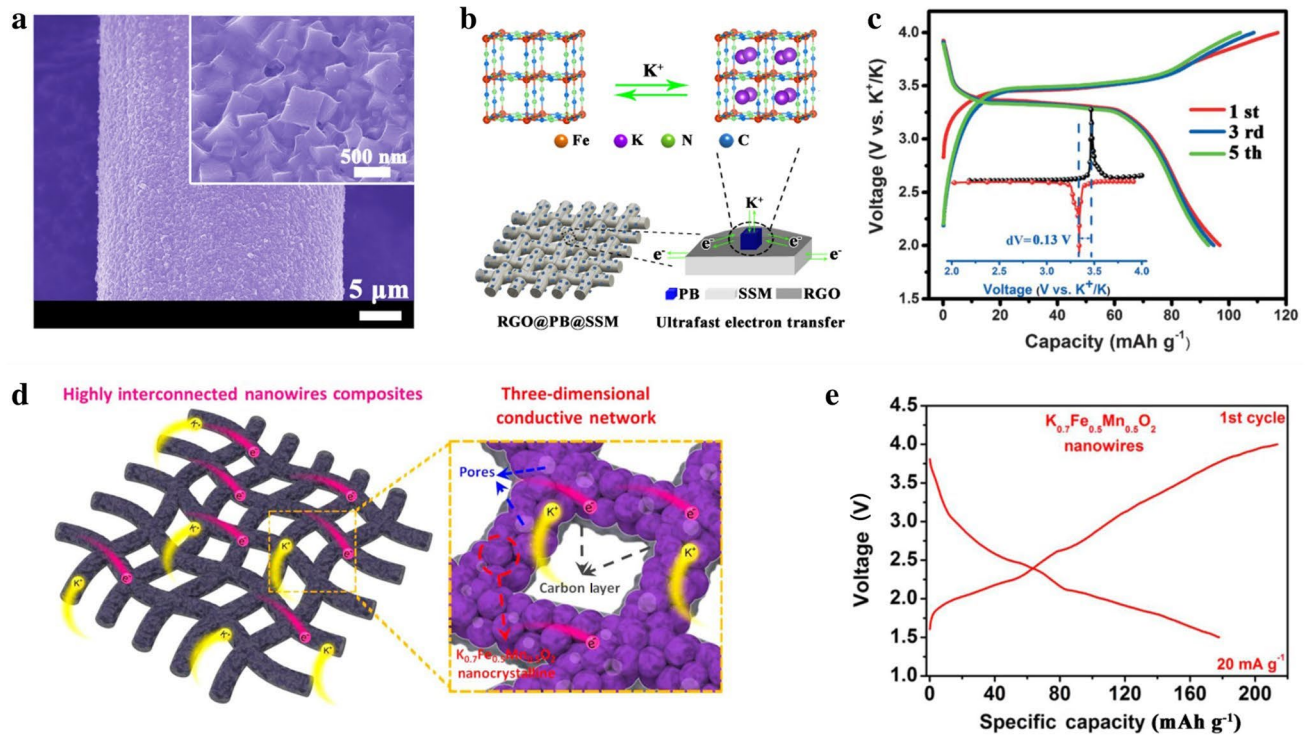

Fig. 13 **a** SEM images of an RGO@PB@SSM electrode. **b** Potassium transport process for the RGO@PB@SSM electrode. **c** Charge/discharge profiles of RGO@PB@SSM electrodes in KIBs. **d** Schematic illustrations of the interconnected $K_{0.7}Fe_{0.5}Mn_{0.5}O_2$ nanowires with three-dimensional continuous electron/K-ion transport pathways. **e** Charge/discharge profiles of the $K_{0.7}Fe_{0.5}Mn_{0.5}O_2$ nanowires in KIBs

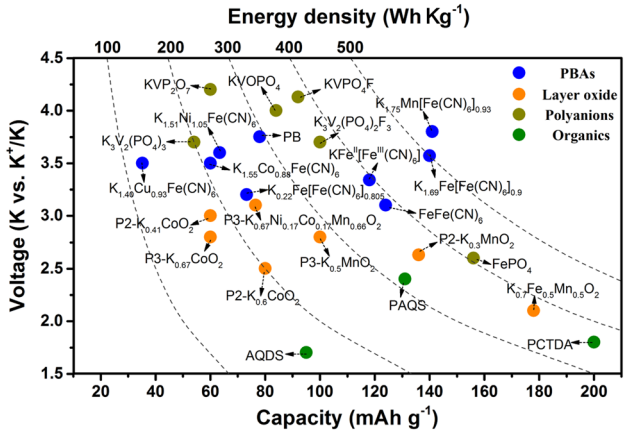

Fig. 14 Reported cathode materials for KIBs and their electrochemical performances, including specific capacity, average working voltage and energy density

application in KIBs. Additionally, PBAs are thermolabile, causing operational issues in batteries in practical settings. Alternatively, layered metal oxides can theoretically deliver higher capacities and better volumetric energy densities due to their closely packed structures. However, in such compact structures, the insertion and diffusion of large-size K ions are less favorable than Li and Na ions, resulting in multistep voltage curves, relatively low reversible capacities and fast capacity fading. Polyanionic compounds are another candidate for large-scale KIBs because of their high working voltages. However, current K-storage performances of polyanionic compounds are unsatisfactory and wide varieties of polyanionic species, including $(PO_4)^{3-}$, $(SO_4)^{2-}$, and $(P_2O_7)^{4-}$, can create many new crystal structures for K-ion storage. Organic materials, which are abundant, environmentally friendly and structurally diverse, are considered to be promising cathodes for future KIBs as well. However, organic materials suffer from issues such as sluggish reaction kinetics and severe material dissolution, all of which need to be resolved for application in KIBs. In addition, due to the high reactivity of potassium metal, the severe decomposition of electrolytes remains ubiquitous in most reported cathode materials. And although fluoroethylene carbonate (FEC) has been reported as an additive to enhance coulombic efficiencies, it could not completely prevent side reactions [99, 100]. Thus, the commercialization of KIBs strongly depends on the research and development of highly stable electrolyte systems.

Overall, because the development of K-storage materials is still in its infancy, most reported KIB cathodes deliver inferior performance compared with LIBs and SIBs.

Table 2 Comparison of the electrochemical performance of reported cathodes in KIBs

Cathodes	Voltage ranges (V)	Cycle performance (current density; cycle number)	Rate capability (current density)
$K_{1.75}Mn[Fe(CN)_6]_{0.93}$ [47]	2~4.5	ca.130 mAh g^{-1} (30 mA g^{-1}; 100)	108 mAh g^{-1} (1 A g^{-1})
$K_{1.69}Fe[Fe(CN)_6]_{0.9}$ [44]	2~4.5	ca. 72 mAh g^{-1} (0.1 A g^{-1}; 300)	120 mAh g^{-1} (0.1 A g^{-1})
$KFe^{II}Fe^{III}(CN)_6$ [42]	2~4.5	73 mAh g^{-1} (0.1 A g^{-1}; 1000)	40.6 mAh g^{-1} (0.5 A g^{-1})
$FeFe(CN)_6$ [43]	1.5~4	93 mAh g^{-1} (0.625 A g^{-1}; 500)	79 mAh g^{-1} (6.25 A g^{-1})
PB [40]	ca. 2.5~4.2	69.1 mAh g^{-1} (8.7 mA g^{-1}; 500)	78.6 mAh g^{-1} (8.7 mA g^{-1})
$K_{0.22}Fe[Fe(CN)_6]_{0.805}$ [41]	2~4	52.4 mAh g^{-1} (0.2 A g^{-1}; 150)	36 mAh g^{-1} (0.4 A g^{-1})
$K_{1.51}Ni_{1.05}Fe(CN)_6$ [49]	2~4.5	ca. 60 mAh g^{-1} (20 mA g^{-1}; 15)	ca. 64 mAh g^{-1} (20 mA g^{-1})
$K_{1.55}Co_{0.88}Fe(CN)_6$ [49]	2~4.5	ca. 38 mAh g^{-1} (20 mA g^{-1}; 15)	ca. 60 mAh g^{-1} (20 mA g^{-1})
$K_{1.40}Cu_{0.93}Fe(CN)_6$ [49]	2~4.5	ca. 29 mAh g^{-1} (20 mA g^{-1}; 15)	ca. 35 mAh g^{-1} (20 mA g^{-1})
$K_{0.7}Fe_{0.5}Mn_{0.5}O_2$ [98]	1.5-4	ca. 60 mAh g^{-1} (1 A g^{-1}; 450)	ca. 52 mAh g^{-1} (1 A g^{-1})
P2-$K_{0.3}MnO_2$ [55]	1.5~4	ca. 80 mAh g^{-1} (27.9 mA g^{-1}; 50)	ca. 15 mAh g^{-1} (1.40 A g^{-1})
P3-$K_{0.5}MnO_2$ [62]	1.5~3.9	ca. 70 mAh g^{-1} (20 mA g^{-1}; 50)	ca. 100 mAh g^{-1} (20 mA g^{-1})
P3-$K_{0.67}Ni_{0.17}Co_{0.17}Mn_{0.66}O_2$ [61]	2~4.3	ca. 66.8 mAh g^{-1} (20 mA g^{-1}; 100)	49 mAh g^{-1} (0.1 A g^{-1})
P2-$K_{0.6}CoO_2$ [57]	1.7~4	ca. 36 mAh g^{-1} (0.1 A g^{-1}; 120)	43 mAh g^{-1} (0.15 A g^{-1})
P2-$K_{0.41}CoO_2$ [56]	2~3.9	ca. 55 mAh g^{-1} (11.8 mA g^{-1}; 30)	ca. 40 mAh g^{-1} (472 mA g^{-1})
P3-$K_{0.67}CoO_2$ [56]	2~3.9	ca. 55 mAh g^{-1} (11.5 mA g^{-1}; 30)	ca. 60 mAh g^{-1} (11.5 mA g^{-1})
$FePO_4$ [68]	1.5~3.5	ca. 109 mAh g^{-1} (4 mA g^{-1}; 50)	156 mAh g^{-1} (4 mA g^{-1})
$K_3V_2(PO_4)F_3$ [71]	2~4.6	90 mAh g^{-1} (20 mA g^{-1}; 180)	20 mAh g^{-1} (0.5 A g^{-1})
$KVPO_4F$ [70]	2~5	ca. 80 mAh g^{-1} (6.65 mA g^{-1}; 30)	92 mAh g^{-1} (6.65 mA g^{-1})
$KVOPO_4$ [70]	2~5	ca. 84 mAh g^{-1} (6.65 mA g^{-1}; 5)	84 mAh g^{-1} (6.65 mA g^{-1})
KVP_2O_7 [72]	2~5	ca. 48.9 mAh g^{-1} (25 mA g^{-1}; 100)	37 mAh g^{-1} (1 A g^{-1})
$K_3V_2(PO_4)_3$ [69]	2.5~4.3	52 mAh g^{-1} (20 mA g^{-1}; 100)	22 mAh g^{-1} (0.2 A g^{-1})
PCTDA [82]	1.5~3.5	90 mAh g^{-1} (50 mA g^{-1}; 200)	75 mAh g^{-1} (0.5 A g^{-1})
PAQS [89]	1.5~3.4	142.5 mAh g^{-1} (20 mA g^{-1}; 50)	190 mAh g^{-1} (20 mA g^{-1})
AQDS [90]	1.5~3	78 mAh g^{-1} (13 mA g^{-1}; 100)	56 mAh g^{-1} (0.65 A g^{-1})

However, with material design improvements and electrolyte optimizations made in the advancement of LIBs and SIBs, KIBs will become a competitive and attractive choice for application in next-generation, large-scale energy storage systems.

Acknowledgements This work was financially supported by the Ministry of Science and Technology of the People's Republic of China (Grant Nos. 2016YFB0100103 and 2017YFA0206704), the National Program on Key Basic Research Project of China (Grant No. 2014CB932300), the Technology and Industry for National Defence of the People's Republic of China (Grant No. JCKY2016130B010), the National Natural Science Foundation of China (Grant Nos. 51522101, 51471075, 51631004 and 51401084) and the China Postdoctoral Science Foundation (Grant No. 2016M601395).

References

1. Armand, M., Tarascon, J.M.: Building better batteries. Nature **451**, 652–657 (2008)
2. Dunn, B., Kamath, H., Tarascon, J.M.: Electrical energy storage for the grid: a battery of choices. Science **334**, 928–935 (2011)
3. Hwang, J.Y., Myung, S.T., Sun, Y.K.: Sodium-ion batteries: present and future. Chem. Soc. Rev. **46**, 3529–3614 (2017)
4. Kundu, D., Talaie, E., Duffort, V., et al.: The emerging chemistry of sodium ion batteries for electrochemical energy storage. Angew. Chem. Int. Edit. **54**, 3431–3448 (2015)
5. Yang, C.J., Jackson, R.B.: Opportunities and barriers to pumped-hydro energy storage in the United States. Renew. Sustain. Energy Rev. **15**, 839–844 (2011)
6. Saidur, R., Rahim, N.A., Hasanuzzaman, M.: A review on compressed-air energy use and energy savings. Renew. Sustain. Energy Rev. **14**, 1135–1153 (2010)
7. Bolund, B., Bernhoff, H., Leijon, M.: Flywheel energy and power storage systems. Renew. Sustain. Energy Rev. **11**, 235–258 (2007)
8. Yang, Z., Zhang, J., Kintner-Meyer, M.C.W., et al.: Electrochemical energy storage for green grid. Chem. Rev. **111**, 3577–3613 (2011)
9. Häupler, B., Wild, A., Schubert, U.S.: Carbonyls: powerful organic materials for secondary batteries. Adv. Energy Mater. **5**, 1402034 (2015)
10. Muldoon, J., Bucur, C.B., Gregory, T.: Quest for nonaqueous multivalent secondary batteries: magnesium and beyond. Chem. Rev. **114**, 11683–11720 (2014)
11. Li, Z., Huang, J., Liaw, B.Y., et al.: A review of lithium deposition in lithium-ion and lithium metal secondary batteries. J. Power Sources **254**, 168–182 (2014)

12. Xu, C., Chen, Y., Shi, S., et al.: Secondary batteries with multivalent ions for energy storage. Sci. Rep. **5**, 14120 (2015)
13. Tarascon, J.M., Armand, M.: Issues and challenges facing rechargeable lithium batteries. Nature **414**, 359–367 (2001)
14. Choi, J.W., Aurbach, D.: Promise and reality of post-lithium-ion batteries with high energy densities. Nat. Rev. Mater. **1**, 16013 (2016)
15. Croguennec, L., Palacin, M.R.: Recent achievements on inorganic electrode materials for lithium-ion batteries. J. Am. Chem. Soc. **137**, 3140–3156 (2015)
16. Slater, M.D., Kim, D., Lee, E., et al.: Sodium-ion batteries. Adv. Funct. Mater. **23**, 947–958 (2013)
17. Speirs, J., Contestabile, M., Houari, Y., et al.: The future of lithium availability for electric vehicle batteries. Renew. Sustain. Energy Rev. **35**, 183–193 (2014)
18. Olivetti, E.A., Ceder, G., Gaustad, G.G., et al.: Lithium-ion battery supply chain considerations: analysis of potential bottlenecks in critical metals. Joule **1**, 229–243 (2017)
19. Pan, H., Hu, Y.S., Chen, L.: Room-temperature stationary sodium-ion batteries for large-scale electric energy storage. Energy Environ. Sci. **6**, 2338–2360 (2013)
20. Kim, H., Kim, J.C., Bianchini, M., et al.: Recent progress and perspective in electrode materials for K-ion batteries. Adv. Energy Mater. **8**, 1702384 (2018)
21. Aurbach, D., Lu, Z., Schechter, A., et al.: Prototype systems for rechargeable magnesium batteries. Nature **407**, 724–727 (2000)
22. Wang, M., Jiang, C., Zhang, S., et al.: Reversible calcium alloying enables a practical room-temperature rechargeable calcium-ion battery with a high discharge voltage. Nat. Chem. **10**, 667–672 (2018)
23. Lin, M.C., Gong, M., Lu, B., et al.: An ultrafast rechargeable aluminium-ion battery. Nature **520**, 325–328 (2015)
24. Okoshi, M., Yamada, Y., Komaba, S., et al.: Theoretical analysis of interactions between potassium ions and organic electrolyte solvents: a comparison with lithium, sodium, and magnesium ions. J. Electrochem. Soc. **164**, 54–60 (2017)
25. Lei, K., Li, F., Mu, C., et al.: High K-storage performance based on the synergy of dipotassium terephthalate and ether-based electrolytes. Energy Environ. Sci. **10**, 552–557 (2017)
26. Wu, X., Leonard, D.P., Ji, X.: Emerging non-aqueous potassium-ion batteries: challenges and opportunities. Chem. Mater. **29**, 5031–5042 (2017)
27. Pramudita, J.C., Sehrawat, D., Goonetilleke, D., et al.: An initial review of the status of electrode materials for potassium-ion batteries. Adv. Energy Mater. **7**, 1602911 (2017)
28. Sultana, I., Rahman, M.M., Chen, Y., et al.: Potassium-ion battery anode materials operating through the alloying–dealloying reaction mechanism. Adv. Funct. Mater. **28**, 1703857 (2018)
29. Komaba, S., Hasegawa, T., Dahbi, M., et al.: Potassium intercalation into graphite to realize high-voltage/high-power potassium-ion batteries and potassium-ion capacitors. Electrochem. Commun. **60**, 172–175 (2015)
30. Jian, Z., Luo, W., Ji, X.: Carbon electrodes for K-ion batteries. J. Am. Chem. Soc. **137**, 11566–11569 (2015)
31. McCulloch, W.D., Ren, X., Yu, M., et al.: Potassium-ion oxygen battery based on a high capacity antimony anode. ACS Appl. Mater. Interfaces **7**, 26158–26166 (2015)
32. Zhang, W., Mao, J., Li, S., et al.: Phosphorus-based alloy materials for advanced potassium-ion battery anode. J. Am. Chem. Soc. **139**, 3316–3319 (2017)
33. Gao, H., Zhou, T., Zheng, Y., et al.: CoS quantum dot nanoclusters for high-energy potassium-ion batteries. Adv. Funct. Mater. **27**, 1702634 (2017)
34. Xie, K., Yuan, K., Li, X., et al.: Superior potassium ion storage via vertical MoS_2 "nano-rose" with expanded interlayers on graphene. Small **13**, 1701471 (2017)
35. Deng, Q., Pei, J., Fan, C., et al.: Potassium salts of para-aromatic dicarboxylates as the highly efficient organic anodes for low-cost K-ion batteries. Nano Energy **33**, 350–355 (2017)
36. Qian, J., Wu, C., Cao, Y., et al.: Prussian blue cathode materials for sodium-ion batteries and other ion batteries. Adv. Energy Mater. **8**, 1702619 (2018)
37. Zhu, Y., Yuan, S., Bao, D., et al.: Decorating waste cloth via industrial wastewater for tube-type flexible and wearable sodium-ion batteries. Adv. Mater. **29**, 1603719 (2017)
38. Mizuno, Y., Okubo, M., Hosono, E., et al.: Electrochemical Mg^{2+} intercalation into a bimetallic CuFe Prussian blue analog in aqueous electrolytes. J. Mater. Chem. A **1**, 13055–13059 (2013)
39. Lipson, A.L., Pan, B., Lapidus, S.H., et al.: Rechargeable Ca-ion batteries: a new energy storage system. Chem. Mater. **27**, 8442–8447 (2015)
40. Eftekhari, A.: Potassium secondary cell based on Prussian blue cathode. J. Power Sources **126**, 221–228 (2004)
41. Zhang, C., Xu, Y., Zhou, M., et al.: Potassium Prussian blue nanoparticles: a low-cost cathode material for potassium-ion batteries. Adv. Funct. Mater. **27**, 1604307 (2017)
42. Chong, S., Chen, Y., Zheng, Y., et al.: Potassium ferrous ferricyanide nanoparticles as a high capacity and ultralong life cathode material for nonaqueous potassium-ion batteries. J. Mater. Chem. A **5**, 22465–22471 (2017)
43. Shadike, Z., Shi, D.R., Cao, M.H., et al.: Long life and high-rate Berlin green $FeFe(CN)_6$ cathode material for a non-aqueous potassium-ion battery. J. Mater. Chem. A **5**, 6393–6398 (2017)
44. He, G., Nazar, L.F.: Crystallite size control of Prussian White analogues for nonaqueous potassium-ion batteries. ACS Energy Lett. **2**, 1122–1127 (2017)
45. Liao, J., Hu, Q., Yu, Y., et al.: A potassium-rich iron hexacyanoferrate/dipotassium terephthalate@carbon nanotube composite used for K-ion full-cells with an optimized electrolyte. J. Mater. Chem. A **5**, 19017–19024 (2017)
46. Xue, L., Li, Y., Gao, H., et al.: Low-cost high-energy potassium cathode. J. Am. Chem. Soc. **139**, 2164–2167 (2017)
47. Bie, X., Kubota, K., Hosaka, T., et al.: A novel K-ion battery: hexacyanoferrate(II)/graphite cell. J. Mater. Chem. A **5**, 4325–4330 (2017)
48. Song, J., Wang, L., Lu, Y., et al.: Removal of interstitial H_2O in hexacyanometallates for a superior cathode of a sodium-ion battery. J. Am. Chem. Soc. **137**, 2658–2664 (2015)
49. Wu, X., Jian, Z., Li, Z., et al.: Prussian white analogues as promising cathode for non-aqueous potassium-ion batteries. Electrochem. Commun. **77**, 54–57 (2017)
50. Ren, W., Qin, M., Zhu, Z., et al.: Activation of sodium storage sites in Prussian blue analogues via surface etching. Nano Lett. **17**, 4713–4718 (2017)
51. Poizot, P., Laruelle, S., Grugeon, S., et al.: Nano-sized transition-metal oxides as negative-electrode materials for lithium-ion batteries. Nature **407**, 496–499 (2000)
52. Wang, Y., Yu, X., Xu, S., et al.: A zero-strain layered metal oxide as the negative electrode for long-life sodium-ion batteries. Nat. Commun. **4**, 2365 (2013)
53. Xu, B., Fell, C.R., Chi, M., et al.: Identifying surface structural changes in layered Li-excess nickel manganese oxides in high voltage lithium ion batteries: a joint experimental and theoretical study. Energy Environ. Sci. **4**, 2223–2233 (2011)
54. Yabuuchi, N., Kajiyama, M., Iwatate, J., et al.: P2-type $Na_x[Fe_{1/2}Mn_{1/2}]O_2$ made from earth-abundant elements for rechargeable Na batteries. Nat. Mater. **11**, 512–517 (2012)

55. Vaalma, C., Giffin, G.A., Buchholz, D., et al.: Non-aqueous K-ion battery based on layered $K_{0.3}MnO_2$ and hard carbon/carbon black. J. Electrochem. Soc. **163**, 1295–1299 (2016)
56. Hironaka, Y., Kubota, K., Komaba, S.: P2-and P3-K_xCoO_2 as an electrochemical potassium intercalation host. Chem. Commun. **53**, 3693–3696 (2017)
57. Kim, H., Kim, J.C., Bo, S.H., et al.: K-ion batteries based on a P2-type $K_{0.6}CoO_2$ cathode. Adv. Energy Mater. **7**, 1700098 (2017)
58. Jiang, J., Li, Y., Liu, J., et al.: Recent advances in metal oxide-based electrode architecture design for electrochemical energy storage. Adv. Mater. **24**, 5166–5180 (2012)
59. Hwang, J.Y., Oh, S.M., Myung, S.T., et al.: Radially aligned hierarchical columnar structure as a cathode material for high energy density sodium-ion batteries. Nat. Commun. **6**, 6865 (2015)
60. Deng, T., Fan, X., Luo, C., et al.: Self-templated formation of P2-type $K_{0.6}CoO_2$ microspheres for high reversible potassium-ion batteries. Nano Lett. **18**, 1522–1529 (2018)
61. Liu, C., Luo, S., Huang, H., et al.: $K_{0.67}Ni_{0.17}Co_{0.17}Mn_{0.66}O_2$: a cathode material for potassium-ion battery. Electrochem. Commun. **82**, 150–154 (2017)
62. Kim, H., Seo, D.H., Kim, J.C., et al.: Investigation of potassium storage in layered P3-type $K_{0.5}MnO_2$ cathode. Adv. Mater. **29**, 1702480 (2017)
63. Gong, Z., Yang, Y.: Recent advances in the research of polyanion-type cathode materials for Li-ion batteries. Energy Environ. Sci. **4**, 3223–3242 (2011)
64. Barpanda, P., Ati, M., Melot, B.C., et al.: A 3.90 V iron-based fluorosulphate material for lithium-ion batteries crystallizing in the triplite structure. Nat. Mater. **10**, 772–779 (2011)
65. Masquelier, C., Croguennec, L.: Polyanionic (phosphates, silicates, sulfates) frameworks as electrode materials for rechargeable Li (or Na) batteries. Chem. Rev. **113**, 6552–6591 (2013)
66. Barpanda, P., Oyama, G., Nishimura, S., et al.: A 3.8-V earth-abundant sodium battery electrode. Nat. Commun. **5**, 4358 (2014)
67. Recham, N., Rousse, G., Sougrati, M.T., et al.: Preparation and characterization of a stable $FeSO_4F$-based framework for alkali ion insertion electrodes. Chem. Mater. **24**, 4363–4370 (2012)
68. Mathew, V., Kim, S., Kang, J., et al.: Amorphous iron phosphate: potential host for various charge carrier ions. NPG Asia Mater. **6**, 138 (2014)
69. Han, J., Li, G.N., Liu, F., et al.: Investigation of $K_3V_2(PO_4)_3$/C nanocomposites as high-potential cathode materials for potassium-ion batteries. Chem. Commun. **53**, 1805–1808 (2017)
70. Chihara, K., Katogi, A., Kubota, K., et al.: $KVPO_4F$ and $KVOPO_4$ toward 4 volt-class potassium-ion batteries. Chem. Commun. **53**, 5208–5211 (2017)
71. Song, W., Cao, X., Wu, Z., et al.: Investigation of the sodium ion pathway and cathode behavior in $Na_3V_2(PO_4)_2F_3$ combined via a first principles calculation. Langmuir **30**, 12438–12446 (2014)
72. Lin, X., Huang, J., Tan, H., et al.: $K_3V_2(PO_4)_2F_3$ as a robust cathode for potassium-ion batteries. Energy Storage Mater. **16**, 97–101 (2018)
73. Park, W.B., Han, S.C., Park, C., et al.: KVP_2O_7 as a robust high-energy cathode for potassium-ion batteries: pinpointed by a full screening of the inorganic registry under specific search conditions. Adv. Energy Mater. **8**, 1703099 (2017)
74. Liang, Y., Tao, Z., Chen, J., et al.: Organic electrode materials for rechargeable lithium batteries. Adv. Energy Mater. **2**, 742–769 (2012)
75. Oyama, N., Tatsuma, T., Sotomura, T.: Organosulfur polymer batteries with high energy density. J. Power Sources **68**, 135–138 (1997)
76. Yao, M., Senoh, H., Yamazaki, S., et al.: High-capacity organic positive-electrode material based on a benzoquinone derivative for use in rechargeable lithium batteries. J. Power Sources **195**, 8336–8340 (2010)
77. Liang, Y., Zhang, P., Yang, S., et al.: Fused heteroaromatic organic compounds for high-power electrodes of rechargeable lithium batteries. Adv. Energy Mater. **3**, 600–605 (2013)
78. Han, X., Chang, C., Yuan, L., et al.: Aromatic carbonyl derivative polymers as high-performance Li-ion storage materials. Adv. Mater. **19**, 1616–1621 (2007)
79. Luo, W., Allen, M., Raju, V., et al.: An organic pigment as a high-performance Cathode for sodium-ion batteries. Adv. Energy Mater. **4**, 1400554 (2014)
80. Wang, H., Yuan, S., Si, Z., et al.: Multi-ring aromatic carbonyl compounds enabling high capacity and stable performance of sodium-organic batteries. Energy Environ. Sci. **8**, 3160–3165 (2015)
81. Zhu, Y., Yang, X., Zhang, X.: Hydronium ion batteries: a sustainable energy storage solution. Angew. Chem. Int. Ed. **56**, 6378–6380 (2017)
82. Chen, Y., Luo, W., Carter, M., et al.: Organic electrode for non-aqueous potassium-ion batteries. Nano Energy **18**, 205–211 (2015)
83. Song, Z.P., Zhan, H., Zhou, Y.H.: Anthraquinone based polymer as high performance cathode material for rechargeable lithium batteries. Chem. Commun. **4**, 448–450 (2009)
84. Zhang, K., Guo, C.Y., Zhao, Q., et al.: High-performance organic lithium batteries with an ether-based electrolyte and 9,10-anthraquinone (AQ)/CMK-3 cathode. Adv. Sci. **2**, 1500018 (2015)
85. Zhang, Y., Huang, Y.S., Yang, G.H., et al.: Dispersion–assembly approach to synthesize three-dimensional graphene/polymer composite aerogel as a powerful organic cathode for rechargeable Li and Na batteries. ACS Appl. Mater. Interfaces **9**, 15549–15556 (2017)
86. Wu, Y.W., Zeng, R.H., Nan, J.M., et al.: Quinone electrode materials for rechargeable lithium/sodium ion batteries. Adv. Energy Mater. **7**, 1700278 (2017)
87. Song, Z.P., Qian, Y.M., Gordin, M.L., et al.: Polyanthraquinone as a reliable organic electrode for stable and fast lithium storage. Angew. Chem. Int. Ed. **54**, 13947–13951 (2015)
88. Wan, W., Lee, H.S., Yu, X.Q., et al.: Tuning the electrochemical performances of anthraquinone organic cathode materials for Li-ion batteries through the sulfonic sodium functional group. RSC Adv. **4**, 19878–19882 (2014)
89. Jian, Z., Liang, Y., Rodríguez-Pérez, I.A., et al.: Poly (anthraquinonyl sulfide) cathode for potassium-ion batteries. Electrochem. Commun. **71**, 5–8 (2016)
90. Zhao, J., Yang, J., Sun, P., et al.: Sodium sulfonate groups substituted anthraquinone as an organic cathode for potassium batteries. Electrochem. Commun. **86**, 34–37 (2018)
91. Zhu, Y.H., Yang, X., Bao, D., et al.: High-energy-density flexible potassium-ion battery based on patterned electrodes. Joule **2**, 736–746 (2018)
92. Jian, Z., Xing, Z., Bommier, C., et al.: Hard carbon microspheres: potassium-ion anode versus sodium-ion anode. Adv. Energy Mater. **6**, 1501874 (2016)
93. Song, H., Li, N., Cui, H., et al.: Enhanced capability and cyclability of SnO_2–graphene oxide hybrid anode by firmly anchored SnO_2 quantum dots. J. Mater. Chem. A **1**, 7558–7562 (2013)
94. Fang, Y., Xiao, L., Ai, X., et al.: Hierarchical carbon framework wrapped $Na_3V_2(PO_4)_3$ as a superior high-rate and extended lifespan cathode for sodium-ion batteries. Adv. Mater. **27**, 5895–5900 (2015)
95. Bruce, P.G., Scrosati, B., Tarascon, J.M.: Nanomaterials for rechargeable lithium batteries. Angew. Chem. Int. Ed. **47**, 2930–2946 (2008)
96. Szczech, J.R., Jin, S.: Nanostructured silicon for high capacity lithium battery anodes. Energy Environ. Sci. **4**, 56–72 (2011)

97. Zhu, Y., Yin, Y., Yang, X., et al.: Transformation of rusty stainless-steel meshes into stable, low-cost, and binder-free cathodes for high-performance potassium-ion batteries. Angew. Chem. Int. Ed. **56**, 7881–7885 (2017)
98. Wang, X., Xu, X., Niu, C., et al.: Earth abundant Fe/Mn-based layered oxide interconnected nanowires for advanced K-ion full batteries. Nano Lett. **17**, 544–550 (2016)
99. Xiao, N., McCulloch, W.D., Wu, Y.: Reversible dendrite-free potassium plating and stripping electrochemistry for potassium secondary batteries. J. Am. Chem. Soc. **139**, 9475–9478 (2017)
100. Jiang, X., Zhang, T., Yang, L., et al.: A Fe/Mn based Prussian blue analogue as a K-rich cathode material for potassium-ion batteries. ChemElectroChem **4**, 2237–2242 (2017)

Yun-Hai Zhu received his B.S. degree in Materials Science and Engineering from Hubei University in 2014. He is currently pursuing a Ph.D. in Materials Science at Jilin University of China. His current interests include design and synthesis of functional materials for sodium-/potassium-ion batteries and flexible energy storage device.

Xu Yang received his Ph.D. degree in 2016 from Jilin University. He is currently working at Changchun Institute of Applied Chemistry as a Postdoctoral Research Associate. He is currently working on the design and synthesis of functional energy storage materials for Na-ion and K-ion batteries.

Tao Sun received his Master's degree in Analytical Chemistry from University of Chinese Academy of Sciences in 2015. He is currently pursuing his Ph.D. in Inorganic Chemistry at Changchun Institute of Applied Chemistry, Chinese Academy of Sciences, under the supervision of Prof. Xin-Bo Zhang. His current interests include the design, synthesis and characterization of novel organic electrode materials for lithium-ion and sodium-ion batteries.

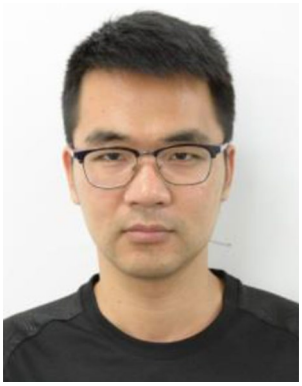

Sai Wang received his B.S. degree of Metallurgical Engineering from University of Science and Technology Liaoning in 2012. He is currently pursuing a Ph.D. in Materials Science at Jilin University of China. His current interests include the synthesis and investigation of low-cost and environmentally friendly electrode materials for lithium-/sodium-ion batteries.

Yin-Lei Zhao received his B.S. degree in Materials Science and Engineering from Jilin University in 2015. He is currently pursuing a Ph.D. under the supervision of Prof. Xin-Bo Zhang at Changchun Institute of Applied Chemistry, Chinese Academy of Sciences. His current research interests include the synthesis and characterization of efficient energy storage materials and their application in ion batteries.

Jun-Min Yan received her Ph.D. degree in inorganic chemistry from Changchun Institute of Applied Chemistry, Chinese Academy of Sciences in 2006. After that, she worked as a JSPS and NEDO fellow at the National Institute of Advanced Industrial Science and Technology, Japan. At the beginning of 2010, she joined the Department of Materials Science and Engineering at Jilin University as a professor of "New Century Excellent Talents in Universities of Ministry of Education of China". Her current research interests focus on the development of new functional materials for (renewable) energy storage and conversion applications.

Xin-Bo Zhang is a Full Professor at Changchun Institute of Applied Chemistry (CIAC), Chinese Academy of Sciences (CAS). He obtained his Ph.D. in Inorganic Chemistry from CIAC and was granted the CAS Presidential Scholarship Award in 2005. From 2005–2009, he worked as a Japan Society for the Promotion of Science (JSPS) postdoctoral fellow (2005–2007) and a New Energy and Industrial Technology Development Organization (NEDO) research associate (2007–2009) at National Institute of Advanced Industrial Science and Technology (AIST), Japan. His interests mainly focus on functional inorganic materials for batteries, fuel cells and electrochemical catalysis.